Recognized as an
American National Standard (ANSI)

IEEE Std 325-1996
(Revision of IEEE Std 325-1986)

IEEE Standard Test Procedures for Germanium Gamma-Ray Detectors

Sponsor

**Nuclear Instruments and Detectors Committee
of the
IEEE Nuclear and Plasma Sciences Society**

Approved 18 October 1996

IEEE Standards Board

Approved 6 January 1997

American National Standards Institute

Abstract: Terminology and standard test procedures for germanium radiation detectors that are used for the detection and high-resolution spectrometry of gamma rays, X rays, and charged particles that produce hole-electron pairs in the crystal lattice are established so they have the same meaning to both manufacturers and users.
Keywords: gamma rays, germanium radiation detectors, X rays

The Institute of Electrical and Electronics Engineers, Inc.
345 East 47th Street, New York, NY 10017-2394, USA

ISBN 1-55937-885-9

IEEE Standards documents are developed within the IEEE Societies and the Standards Coordinating Committees of the IEEE Standards Board. Members of the committees serve voluntarily and without compensation. They are not necessarily members of the Institute. The standards developed within IEEE represent a consensus of the broad expertise on the subject within the Institute as well as those activities outside of IEEE that have expressed an interest in participating in the development of the standard.

Use of an IEEE Standard is wholly voluntary. The existence of an IEEE Standard does not imply that there are no other ways to produce, test, measure, purchase, market, or provide other goods and services related to the scope of the IEEE Standard. Furthermore, the viewpoint expressed at the time a standard is approved and issued is subject to change brought about through developments in the state of the art and comments received from users of the standard. Every IEEE Standard is subjected to review at least every five years for revision or reaffirmation. When a document is more than five years old and has not been reaffirmed, it is reasonable to conclude that its contents, although still of some value, do not wholly reflect the present state of the art. Users are cautioned to check to determine that they have the latest edition of any IEEE Standard.

Comments for revision of IEEE Standards are welcome from any interested party, regardless of membership affiliation with IEEE. Suggestions for changes in documents should be in the form of a proposed change of text, together with appropriate supporting comments.

Interpretations: Occasionally questions may arise regarding the meaning of portions of standards as they relate to specific applications. When the need for interpretations is brought to the attention of IEEE, the Institute will initiate action to prepare appropriate responses. Since IEEE Standards represent a consensus of all concerned interests, it is important to ensure that any interpretation has also received the concurrence of a balance of interests. For this reason, IEEE and the members of its societies and Standards Coordinating Committees are not able to provide an instant response to interpretation requests except in those cases where the matter has previously received formal consideration.

Comments on standards and requests for interpretations should be addressed to:

Secretary, IEEE Standards Board
445 Hoes Lane
P.O. Box 1331
Piscataway, NJ 08855-1331
USA

Note: Attention is called to the possibility that implementation of this standard may require use of subject matter covered by patent rights. By publication of this standard, no position is taken with respect to the existence or validity of any patent rights in connection therewith. The IEEE shall not be responsible for identifying patents for which a license may be required by an IEEE standard or for conducting inquiries into the legal validity or scope of those patents that are brought to its attention.

Introduction

(This introduction is not part of IEEE Std 325-1996, IEEE Standard Test Procedures for Germanium Gamma-Ray Detectors.)

IEEE Std 325-1996 provides standard test procedures for germanium gamma-ray detectors for ionizing radiation. It is a revision of IEEE Std 325-1986, updated to bring it into line with current practices and technology. The revision was approved by the Nuclear Instruments and Detectors Committee (NIDC) of the IEEE Nuclear and Plasma Sciences Society and by the Accredited Standards Committee on Nuclear Instrumentation of the American National Standards Institute. The previous revision of this standard, published as ANSI/IEEE 325-1986, combined and updated ANSI/IEEE Std 325-1971, ANSI/IEEE Std 645-1987, and ANSI/IEEE Std 680-1980.

Companion documents are IEEE Std 300-1988 (Reaff 1993), IEEE Standard Test Procedures for Semiconductor Charged-Particle Detectors (ANSI); IEEE Std 301-1988 (Reaff 1993), IEEE Standard Test Procedures for Amplifiers and Preamplifiers Used with Detectors of Ionizing Radiation (ANSI); and IEEE Std 759-1984 (Reaff 1990), IEEE Test Procedures for Semiconductor X-Ray Energy Spectrometers (ANSI).

At the time it approved this standard, the NIDC had the following membership:

Sanford Wagner, *Chair* **Louis Costrell,** *Secretary*

David J. Allard
Martin L. Bauer
Joseph G. Bellian
William M. Bugg
Christopher Cox
Larry Darken
W. Kenneth Dawson
John Detko
Edward Fairstein
Ronald M. Keyser
Frederick A. Kirsten
Glenn F. Knoll
Hobard W. Kraner
G. Laurie Miller
Dennis E. Persyk
Paul L. Phelps
Donald E. Stilwell
Kenneth L. Swinth
James H. Trainor
Michael Unterweger
John Walter

Edward Fairstein and Sanford Wagner served as project leaders for the development of this standard.

The Accredited Standards Committee on Radiation Instrumentation, N42, which reviewed and approved this document, had the following membership at the time of approval:

Louis Costrell, *Chair* **Luigi Napoli,** *Secretary*

Organization Represented	*Name of Representative*
American Conference of Governmental Industrial Hygienists	Jesse Lieberman
Health Physics Society	George Campbell
	Joseph Stencel *(Alt.)*
Institute of Electrical and Electronics Engineers	Louis Costrell
	Julian Forster *(Alt.)*
	Anthony J. Spurgin *(Alt.)*
Lawrence Berkeley Laboratory	Edward J. Lampo
Lawrence Livermore National Laboratory	Paul L. Phelps
Massachusetts Institute of Technology, Bates Linear Accelerator Center	Frank X. Masse
Oak Ridge National Laboratory	Charles L. Britton
Pacific Northwest Laboratories	Kenneth L. Swinth
U.S. Department of the Army	Edward Groeber
U.S. Department of Commerce, National Institute of Standards and Technology	Louis Costrell
	Michael Unterweger *(Alt.)*
U.S. Department of Energy, OHER/PCSRD	Gerald Goldstein
U.S. Federal Emergency Management Agency	Carl R. Siebentritt
Individual Members	Joseph G. Bellian
	Ernesto A. Corte
	Morgan Cox
	John M. Gallagher
	Jack M. Selby
	Al N. Tschaeche
	Edward J. Vallario
	Lee J. Wagner
	Sanford Wagner

When the IEEE Standards Board approved this standard on 18 October 1996, it had the following membership:

Donald C. Loughry, *Chair* **Richard J. Holleman,** *Vice Chair*
Andrew G. Salem, *Secretary*

Gilles A. Baril
Clyde R. Camp
Joseph A. Cannatelli
Stephen L. Diamond
Harold E. Epstein
Donald C. Fleckenstein
Jay Forster*
Donald N. Heirman
Ben C. Johnson
E. G. "Al" Kiener
Joseph L. Koepfinger*
Stephen R. Lambert
Lawrence V. McCall
L. Bruce McClung
Marco W. Migliaro
Mary Lou Padgett
John W. Pope
Jose R. Ramos
Arthur K. Reilly
Ronald H. Reimer
Gary S. Robinson
Ingo Rüsch
John S. Ryan
Chee Kiow Tan
Leonard L. Tripp
Howard L. Wolfman

*Member Emeritus

Also included are the following nonvoting IEEE Standards Board liaisons:

Satish K. Aggarwal
Alan H. Cookson
Chester C. Taylor

Kristin M. Dittmann
IEEE Standards Project Editor

Contents

CLAUSE PAGE

IEEE Standard Test Procedures for Germanium Gamma-Ray Detectors

1. Overview

1.1 Scope

This standard applies to germanium radiation detectors that are used for the detection and high-resolution spectrometry of gamma rays, X rays, and charged particles that produce hole-electron pairs in the crystal lattice. Included are detector endcap and reentrant (Marinelli) beaker standards.

Measurements that depend upon phonon production are outside the scope of this standard.

1.2 Purpose

The purpose of this standard is to establish terminology and standard test procedures so they have the same meaning to both manufacturers and users.

Not all tests described in this standard are mandatory, but tests that are used to specify performance shall be performed in accordance with the procedures described herein.

2. References

This standard shall be used in conjunction with the following publications:

IEEE Std 194-1977, IEEE Standard Pulse Terms and Definitions.[1]

IEEE Std 300-1988 (Reaff 1993), IEEE Standard Test Procedures for Semiconductor Charged-Particle Detectors (ANSI).

IEEE Std 301-1988 (Reaff 1993), IEEE Standard Test Procedures for Amplifiers and Preamplifiers Used with Detectors of Ionizing Radiation (ANSI).

IEEE Std 759-1984 (Reaff 1990), IEEE Test Procedures for Semiconductor X-ray Energy Spectrometers (ANSI).

[1]IEEE Std 194-1977 has been withdrawn; however, copies can be obtained from Global Engineering, 15 Inverness Way East, Englewood, CO 80112-5704, USA, tel. (303) 792-2181. Other IEEE publications are available from the Institute of Electrical and Electronics Engineers, 445 Hoes Lane, P.O. Box 1331, Piscataway, NJ 08855-1331, USA.

IEEE Std 1160-1993, IEEE Standard Test Procedures for High-Purity Germanium Crystals for Radiation Detectors (ANSI).

DOE Report DOE/ER-0457T, Standard NIM Instrumentation System (May 1990).[2]

3. Definitions, symbols, and abbreviations and acronyms

3.1 Definitions

Of the following definitions, several are “distributed”; that is, terms are used that are themselves defined in other definitions in this clause.

3.1.1 active region: A region of a detector in which charge created by ionizing radiation contributes significantly to the output signal.

3.1.2 amplifier noise: *See:* noise referred to the input.

3.1.3 amplifier shaping time: A nonspecific indication of the shaped-pulse width issuing from a linear pulse amplifier. *See:* shaping index.

3.1.4 amplifier time constant: A misnomer for the width of the shaped pulse issuing from a linear pulse amplifier. *See:* shaping index.

3.1.5 avalanche breakdown: A breakdown caused by the cumulative multiplication of charge carriers through electric-field-induced impact ionization.

3.1.6 background (ambient): The spectrum of X or gamma rays originating from materials other than the radionuclide being measured.

3.1.7 background (under a peak): The background from all sources under a peak being measured, including Compton and degraded-energy counts from higher energy and ambient background events.

3.1.8 ballistic deficit: The loss in signal amplitude that occurs when the charge collection time in a detector is a significant fraction of the amplifier’s differentiating time constant.

3.1.9 band gap: The energy difference between the bottom of the conduction band and the top of the valence band.

3.1.10 baseline (of an electrical pulse): The average of the levels from which a pulse departs and to which it returns in the absence of an overlapping pulse (IEEE Std 194-1977[3]).

3.1.11 baseline restorer (BLR): A circuit that rapidly restores the baseline following an amplifier’s output pulse (or train of pulses) to the level that existed before the pulse.

3.1.12 bias, detector: The voltage applied to a detector to produce the electric field that sweeps out the signal charge.

3.1.13 bias resistor: The resistor through which the bias voltage is applied to a detector.

[2]Available from Louis Costrell, NIM Committee Chairman, National Institute of Standards and Technology, Radiation Physics Division, or from the National Technical Information Service, U.S. Dept. of Commerce, Springfield, VA 22161.

[3]Information on references can be found in Clause 2.

3.1.14 bipolar pulse: A signal pulse having two lobes, one above and the other below the baseline (IEEE Std 194-1977). When produced by a linear filter network, the two lobes have the same area but not necessarily the same peak amplitude.

3.1.15 breakdown: A phenomenon occurring in a reverse-biased semiconductor diode that appears as an increase in noise, reverse current, or both when the bias is increased beyond a certain value.

3.1.16 breakdown voltage: The voltage measured at a specified current in the breakdown region.

3.1.17 capacitance, detector: The small-signal electrical capacitance measured between terminals of the detector under specified conditions of bias and frequency.

3.1.18 channeling, lattice: A phenomenon that results in a crystallographic directional dependence of the rate of energy loss of ionizing particles.

3.1.19 channel, surface: A thin region at a semiconductor surface of p- or n-type conductivity created by the action of an electric field (for example, that due to trapped surface charge).

3.1.20 charge carrier (abbreviation: carrier): A mobile electron or hole.

3.1.21 charge collection time: The time interval after the passage of an ionizing particle for the integrated current flowing between the terminals of the detector to increase from 10% to 90% of its final value.

3.1.22 charge-sensitive preamplifier: An amplifier preceding the main amplifier in which the output amplitude is proportional to the charge injected at the input. *See:* voltage-sensitive preamplifier.

3.1.23 constant-fraction discriminator: A discriminator in which the threshold is set at a fixed *fraction* of the input signal (instead of to a fixed *amplitude*). This is one of a class of timing discriminators.

3.1.24 contact, ion implanted: A detector contact consisting of a junction made by the process of ion implantation. *See:* ion implantation.

3.1.25 contact, ohmic: A purely resistive contact that has a linear voltage-current characteristic throughout its entire operating range.

3.1.26 contact, Schottky-barrier: A metal-semiconductor contact structure in which the rectification that occurs is heavily influenced by the difference in the work functions of the materials. The contacts frequently consist of an interfacial metal/semiconductor compound such as a silicide.

3.1.27 contact, surface-barrier: A metal-insulator-semiconductor contact structure in which the rectification properties are dominated or heavily influenced by charge trapped at the interfaces and in the insulator.

3.1.28 *CR* differentiator: A high-pass electrical filter section consisting of a capacitor in series with the signal path followed by a resistor across the path.

3.1.29 crest factor (of an rms voltmeter): The highest ratio of peak-to-rms voltage that can be applied to an ac voltmeter before overload sets in. The crest factor may depend on the full-scale setting of the voltmeter.

3.1.30 $(CR)^m$–$(RC)^n$ shaping: In an amplifier, the pulse shape produced by m *CR* high-pass filter sections (differentiators) in conjunction with n *RC* low-pass filter sections (integrators), all with the same time constant. If the input signal is a step function and no other high-pass sections are in the signal path, the pulse shape is unipolar if $m = 1$, bipolar if $m = 2$. For unipolar pulses, the waveform is described by $Kt^n e^{-t/\tau}$ where K is a constant, t is time, and τ is the time constant of the differentiator.

3.1.31 crossover time (of a bipolar pulse): The instant at which the transition between the two lobes passes through a designated level (usually the baseline). At this level, the timing with respect to the initiating events is nearly invariant with pulse amplitude.

3.1.32 dead layer: In a semiconductor detector, a layer (frequently associated with a contact region) in which no significant part of the energy lost by photons or particles can contribute to the resulting signal.

3.1.33 decay time constant: In the absence a low-pass network preceding the point of observation, the time for a single-exponential waveform to decay to the fraction 1/*e* of its original amplitude.

3.1.34 depletion region: A region in which the mobile charge-carrier density is insufficient to neutralize the net fixed charge density of donors and acceptors. In a diode-type semiconductor radiation detector, the depletion region is the active (sensitive) region.

3.1.35 depletion voltage: The voltage at which a junction detector becomes fully depleted.

3.1.36 detector, coaxial: A detector in which all or part of the two electrical contacts on the detector element are substantially coaxial. Typically one end of each contact configuration is closed (closed-ended coaxial detector), but both ends may be open (open-ended coaxial detector).

3.1.37 detector, coaxial, conventional-electrode geometry: A coaxial detector in which the outer contact is an n-type layer.

3.1.38 detector, coaxial, reverse-electrode geometry: A coaxial detector in which the outer contact is a p-type layer.

3.1.39 detector, differential (*dE*/*dx*): *See:* detector, transmission.

3.1.40 detector, diffused-junction: A semiconductor detector in which the rectifying junction is produced by diffusion of acceptor (p) or donor (n) defects.

3.1.41 detector element: The semiconductor crystal including its contacts.

3.1.42 detector, germanium gamma-ray: A complete assembly, including the detector element, cryostat, integral preamplifier, and high-voltage filter. *See:* detector element.

3.1.43 detector, p-i-n: A detector consisting of an intrinsic or nearly intrinsic region between a p- and an n-region.

3.1.44 detector, position-sensitive: A detector in which the centroid of the area of impact of ionizing radiation can be determined from the signals issuing from its terminals. Depending on the design, position sensing can be in one or more dimensions.

3.1.45 detector, semiconductor radiation: A semiconductor device in which the production and motion of excess free carriers is used for the detection and measurement of incident particles or photons.

3.1.46 detector, Schottky-barrier: A semiconductor radiation detector in which the blocking contact is of the Schottky-barrier type.

3.1.47 detector, surface barrier: A radiation detector in which the principal rectifying junction is a surface-barrier contact.

3.1.48 detector, totally depleted: A detector in which the thickness of the depletion region is essentially equal to the thickness of the semiconductor material.

3.1.49 detector, transmission: A detector that is thin compared with the range of the incident particle and in which the entrance and exit dead layers are thin compared with the thickness of the detector.

3.1.50 detector, well-type coaxial: A coaxial detector that is mounted and encapsulated in such a way that a radioactive sample can be placed within the inner cylindrical electrode such that the sample is essentially surrounded by active detector material.

3.1.51 differentiator: A high-pass filter network in which the waveform of the output signal approximates the mathematical derivative of the input waveform.

3.1.52 discriminator: A circuit having a threshold below which signals applied to the input will not cause an output signal and above which the input signal will trigger an output having an amplitude independent of the input signal height.

3.1.53 energy count-rate product: Obsolete. *See:* energy rate limit.

3.1.54 energy rate: The average energy per event times the number of events per second.

3.1.55 energy rate limit: In a preamplifier dc-coupled to a detector, the highest energy rate in units of MeV per second that causes no more than a specified fraction of the pulses (usually 1%) to overload the preamplifier.

3.1.56 energy resolution: The full width at half maximum of a peak in a spectrum, after subtracting the background under the peak; expressed in units of energy, usually keV; or as a percentage of the energy corresponding to that peak.

3.1.57 equivalent noise resistance referred to the input of an amplifier: This is an ambiguous term; the qualifiers "series" or "parallel" must be specified. *See:* equivalent series (parallel) noise resistance referred to the input of an amplifier.

3.1.58 equivalent series (parallel) noise resistance referred to the input of an amplifier: In a hypothetically noise-free amplifier, the value of resistor that, when connected in series with (shunted across) its input, will produce the same output noise spectrum as is observed in the real amplifier. The gain and bandwidth of the real and hypothetical amplifiers must be the same for this definition to be valid.

3.1.59 fall time t_f (of a pulse): The interval on the last transition between the 90% and 10% points (unless other levels are specified) with respect to peak height. *See*: transition.

3.1.60 full width at half maximum (FWHM): The full width of a distribution measured at half the maximum ordinate. For a normal distribution, FWHM = $2 \cdot (2 \ln 2)^{1/2} = 2.355$ times the standard deviation, σ.

3.1.61 gated integrator: A circuit for obtaining an output pulse with an amplitude proportional to the integral of the input signal over a definite time interval.

3.1.62 geometry, detector element: The physical configuration of a detector element. *See:* detector element.

3.1.63 high-purity germanium (HPGe): Germanium with a low, net electrically active, uncompensated defect concentration usually less than $\approx 10^{10}$ cm^{-3}.

3.1.64 inactive region (of a semiconductor radiation detector): A region of a detector in which charge created by ionizing radiation does not contribute significantly to the output signal.

3.1.65 integrated pulse: In the absence of qualifiers (such as "true integration"), a pulse that has passed through one or more low-pass networks ("integrators").

3.1.66 intrinsic semiconductor: A semiconductor containing an equal number of free holes and electrons throughout its volume. The term *intrinsic germanium* often is used incorrectly to describe high-purity germanium.

3.1.67 ion implantation: A process in which a beam of energetic ions incident upon a solid results in the imbedding of those ions into the material.

3.1.68 junction: The transition boundary between semiconductor regions of different electrical properties (for example, $n - n,^{+}$ $p - n$, $p - p^{+}$ semiconductors, or between a metal and a semiconductor).

3.1.69 junction, rectifying: A region between two materials, typically n-type or p-type semiconductors, or between a metal and a semiconductor, arranged to provide a very low resistance to current flow in one direction and a very high resistance to current flow in the opposite direction.

3.1.70 leakage current: In the absence of external ionizing radiation and at the operating bias, the total current flowing through or across the surface of the detector element.

3.1.71 line (in a spectrum): A sharply peaked portion of a spectrum that represents a specific feature of the incident radiation, usually the full energy of a monoenergetic X ray, gamma ray, or charged particle.

3.1.72 linear filtering: Pulse shaping in which the filter response does not change with time. [$CR–(RC)^{n}$ shaping is an example of linear filtering.]

3.1.73 main amplifier (shaping amplifier): The section of amplifier following the preamplifier that contains the pulse-shaping networks (filter networks). These networks optimize the signal-to-noise ratio in the amplifying chain.

3.1.74 Marinelli beaker: A reentrant (inverted well) beaker that can be fitted over a detector endcap for the purpose of holding a radioactive sample in a configuration that surrounds a major portion of the detector.

3.1.75 microphonics, microphonic noise: Electrical noise caused by mechanical or audio-induced vibration of the detector assembly.

3.1.76 NIM: A standardized modular instrumentation system consisting of NIM Modules and NIM Bins as defined in DOE Report DOE/ER-0457T.

3.1.77 NIM Bin: A mounting unit or housing for NIM Modules that conforms to the requirements of DOE Report DOE/ER-0457T. It includes bussed connectors at the rear that mate with connectors on the modules to provide the modules with power.

3.1.78 NIM Module, NIM Instrument: A modular functional unit or instrument that mounts in a NIM Bin and conforms to the requirements of DOE Report DOE/ER-0457T.

3.1.79 noise linewidth: The contribution of electrical noise to the width of a spectral peak. (Electrical noise adds to the peak width in quadrature.)

3.1.80 noise referred to the input (of an amplifier): The electronic noise level at the input of a hypothetically noise-free amplifier that would produce the same noise as measured at the point of observation in the actual amplifier. This definition is implied when the term “amplifier noise” is used without qualifications.

3.1.81 parallel noise (of a device): Electrical noise that can be attributed to a hypothetical white noise generator connected in parallel with the input of the device.

3.1.82 peak (in a spectrum): *See:* line (in a spectrum).

3.1.83 peaking time t_p (of a pulse): The interval between the 1% point on the first transition, with respect to the peak height, and the top center line (see transition and top centerline).

3.1.84 preamplifier: The input section of an amplifier chain, usually located as close to the detector element as possible.

3.1.85 preamplifier, pulsed optical feedback: An integrating preamplifier in which the charge that accumulates on the feedback capacitor is periodically reset by a pulse of light incident on a photosensitive element, such as the gate of the n-p junction of the input FET.

3.1.86 pulse duration (at the baseline): The width of a pulse measured close to the baseline, typically at 1% of the peak height ($t_{.01}$).

3.1.87 quasi-Gaussian pulse shape: A pulse shape approximated by the curve of a normal or Poisson distribution. In this standard, four or more integrators shall be used in producing the pulse. *See:* integrated pulse.

3.1.88 quasi-triangular pulse shape: A pulse shape approximated by a triangle with a truncated top. Such a shape can be obtained from a $CR-(RC)^n$ or sine^n network by summing appropriate signal fractions from the n integrating sections. *See:* $CR-(RC)^n$ shaping and sine^n shaping.

3.1.89 RC integrator: A low-pass electrical filter section consisting of a resistor in series with the signal path followed by a capacitor across it.

3.1.90 resolution: *See:* energy resolution.

3.1.91 rise time t_r (of a pulse): The interval on the first transition between the 10% and 90% points, with respect to peak height, unless other levels are specified. *See:* transition.

3.1.92 semiconductor: Material in which the conductivity is due to charge carriers of both signs (electrons and holes), is normally in the range between metals and insulators, and in which the charge-carrier density can be changed by external means.

3.1.93 semiconductor, compensated: A semiconductor in which one type of impurity or imperfection (for example, donor) partially cancels the electric effects of the other type of impurity or imperfection (for example, acceptor).

3.1.94 series noise (of a device): The fraction of electrical noise that can be attributed to a hypothetical white noise generator connected in series with the input of the device.

3.1.95 shaped pulse: In this standard, the pulse shape produced by passing the output signal from the preamplifier (approximately a step function) through the pulse-shaping network in the main amplifier (shaping amplifier).

3.1.96 shaping amplifier: *See:* main amplifier.

3.1.97 shaping index: In a main amplifier, the width of the shaped unipolar pulse measured at 50% of its peak height, designated as $t_{0.5}$.

3.1.98 shaping time (in an amplifier): *See:* amplifier shaping time.

3.1.99 signal-to-noise ratio: In this standard, “signal” refers to peak signal, and “noise” refers to rms noise.

3.1.100 sine^n shaping: In an amplifier, the pulse shape produced by one CR high-pass filter section (differentiator) followed by n RC low-pass filter sections (integrators), all with different time constants, but follow-

ing a particular pattern related to the differentiating time constant τ. If the input signal is a step function and no other high-pass sections are in the signal path, the pulse shape is unipolar and is described by $Ke^{-3t/\tau}\sin^n(t/\tau)$, where K is a constant, t is time, and τ is the time constant of the differentiator.

3.1.101 skewing factor $S_{0.1}$ or $S_{.02}$ (of a peak): The ratio (FW.1M)/(1.823 FWHM) or (FW.02M)/(2.376 FWHM). For an ideal Gaussian shape, the factors are 1.000. If the peak is wider at FW.1M or FW.02M than it should be relative to FWHM, the factors are >1.000. (For a perfect Gaussian peak, FW.1M/FWHM = $[(\ln 0.1)/(\ln 0.5)]^{1/2}$ = 1.823 and FW.02M/FWHM = $[(\ln 0.02)/(\ln 0.5)]^{1/2}$) = 2.376).

3.1.102 source, radioactive: A radionuclide prepared in a form convenient for use in testing a detector or spectrometer.

3.1.103 space-charge generation (in a semiconductor radiation detector): The thermal generation of free charge carriers in the depletion region.

3.1.104 space-charge region: *See:* depletion region.

3.1.105 spectrum, energy: A differential distribution of the intensity of radiation as a function of energy.

3.1.106 straggling, energy: The random fluctuations in energy loss whereby those particles having the same initial energy lose different amounts of energy when traversing a given thickness of matter. (This process may lead to the broadening of spectral lines.)

3.1.107 timing discriminator: A class of discriminators in which the initiation of the output signal is keyed to the instant when the input signal crosses the discriminator threshold. *See:* discriminator, constant-fraction discriminator.

3.1.108 time-variant filtering: Pulse shaping in which the filter response varies with time.

3.1.109 top center line (of a pulse): In a peaked pulse, the ordinate that passes through the peak; in a flat-topped pulse, the ordinate that bisects the nominally flat-topped region (IEEE Std 194-1977).

3.1.110 transistor reset preamplifier: An integrating preamplifier in which the charge that accumulates on the feedback capacitor is drained off through a transistor when the charge exceeds a predetermined value.

3.1.111 transition (of a pulse): The region of a pulse in which a major change in amplitude occurs, such as at the leading edge (first transition) or final trailing edge (last transition) (IEEE Std 194-1977).

3.1.112 unipolar pulse: A signal pulse having a single lobe above (or below) the baseline.

3.1.113 voltage-sensitive preamplifier: An amplifier, preceding the main amplifier, in which the amplitude of the output signal is proportional to the signal voltage appearing across the capacitance that exists at the input of the preamplifier. *See:* charge-sensitive preamplifier.

3.1.114 walk (in a pulse): The change in the timing (with respect to the initiating event) of a reference point on a pulse caused by a change in pulse amplitude.

3.2 Symbols

B_Δ	The background counts-per-channel difference between the low- and high-energy sides of a peak
B_H	The average background counts per channel on the high-energy side of a peak
B_L	The average background counts per channel on the low-energy side of a peak
C	The electrical capacitance

C_c	The calibrated capacitor that couples a pulse generator to a circuit under test
C_f	The feedback capacitance in the charge-sensitive loop of a preamplifier
C_t	The total capacitance at the input of a preamplifier
Δ	The full width at half maximum (FWHM) of a spectral peak
ΔE_O	FWHM, expressed in units of energy, due to all factors other than electronic noise
ΔE_S	FWHM, expressed in units of energy, derived in spectral energy resolution measurement
ΔE_T	FWHM, expressed in units of energy, due to the combined effects of detector and amplifier noise
ΔN_O	FWHM, expressed in channels, due to all factors other than electronic noise
ΔN_S	FWHM, expressed in channels, of a spectral peak used for energy resolution determination
ΔN_T	FWHM, expressed in channels, due to the combined effect of detector and amplifier noise
E, E_i	The energy of a particle or radiation (or energy of a specific value, E_i, where i is an integer, 1, 2,…)
e	The charge of the electron
ε	The average energy required to form one hole-electron pair in a semiconductor detector
I	The electric current
N_c	The number of counts in channel c of a spectrum where channel c lies within a specified energy range within the Compton continuum
N_X	The number of counts in channel X of a spectrum
$\hat{N}$	The number of counts in the peak channel $\hat{X}$ of a spectrum
Q	The electric charge
R_f	The feedback resistor in the charge-sensitive loop of a preamplifier
$S_{0.1}$	The skewing factor at FW.1M = (FW.1M)/(1.823 FWHM)
$S_{.02}$	The skewing factor at FW.02M = (FW.02M)/(2.376 FWHM)
$t_{.01}$	The pulse width at 1% of the peak pulse height
$t_{0.5}$	The pulse width at half maximum
t_r	The pulse rise time (10–90% of its peak value)
τ	The time constant
τ_d	The time constant for the decay of a pulse
X, X_i	The channel number, and that number corresponding to energy E_i
$\hat{X}$	The interpolated channel number corresponding to the maximum of a monoenergetic spectral peak

3.3 Abbreviations and acronyms

ADC	analog-to-digital converter
BLR	baseline restorer
c/s	counts per second
CSP	charge-sensitive preamplifier
ERL	energy rate limit in units of megaelectronvolts per second
FET	field-effect transistor
FoM	figure of merit
FWHM	full width of a peak at half its maximum height
FW.1M	full width of a peak at one-tenth its maximum height
FW.02M	full width of a peak at one-fiftieth of its maximum height
Ge(Li)	lithium-drifted germanium
HPGe	high-purity germanium
LN	liquid nitrogen
MCA	multichannel pulse-height analyzer
MDA	minimum detectable activity
NaI(Tl)	thallium-activated sodium iodide
NIM	nuclear instrument module

P/C	peak-to-Compton ratio
rms	root-mean-square
SNR	ratio of the peak signal to the rms noise

4. General

4.1 The interaction of gamma rays with matter

Gamma rays interact with matter through three principal processes: the photoelectric effect, the Compton effect, and pair production.

4.1.1 Photoelectric effect

The photoelectric effect takes place when an incident photon transfers its entire energy to a bound electron in an atom, resulting in the ejection of that electron. Its kinetic energy equals the photon energy less the electron binding energy. The cross section for the photoelectric effect increases approximately as $Z^{4.5}$ where Z is the atomic number of the absorber, and decreases approximately as E^3 where E is the photon energy.

4.1.2 Compton effect

The Compton effect may be considered as an elastic collision of a photon with an atomic electron. The electron is ejected from the atom, and the photon is scattered with reduced energy. The scattered photon may then repeat the scattering process, be fully absorbed, or escape from the absorber. The cross section for the Compton effect decreases with increasing energy, but much less rapidly than for the photoelectric effect.

Compton-scattered photons that escape the detector element are lost to the detection process. Those remaining behind produce counts in the energy region below the photopeak, contributing to a continuous background (not to be confused with the natural background; see 4.1.6). The problem is particularly serious in environmental studies of low-level radiation consisting of spectra with many peaks, because each of the higher energy lines adds to the background distribution in the energy region below it, making the measurements increasingly difficult as the search moves toward lower energies. The Compton background is the limiting factor in establishing the minimum detectable activity (MDA) in a given measuring time, or in determining the number of samples that can be processed to a specified MDA.

Generally, large detector elements exhibit lower Compton background than small ones (see 4.6).

4.1.3 Pair production

Pair production takes place when the energy of a photon is converted into an electron and a positron in the presence of a nearby nucleus. This process requires a minimum energy of 1.02 MeV, which is the sum of the rest mass energies of the electron and the positron. Above this energy the cross section for pair production increases to a maximum, then decreases due to screening effects.

The linear attenuation coefficients for silicon and germanium are shown in Figure 4-1. In all of these absorption processes the energy of incident photons is transferred to one or more electrons. These rapidly lose their energy in the absorber material, largely through Coulomb interactions that produce a cascade of free electrons and holes. Energy from these processes also produces phonons, the production of which is a competing form of energy loss that adds to the statistical fluctuation in the amplitudes of recorded events but not to their average magnitude. In this standard, the interest is in the events arising from those interactions of gamma rays with matter that produce ionization in the form of electron-hole pairs, the average quantity being directly proportional to the absorbed energy of the incident photon.

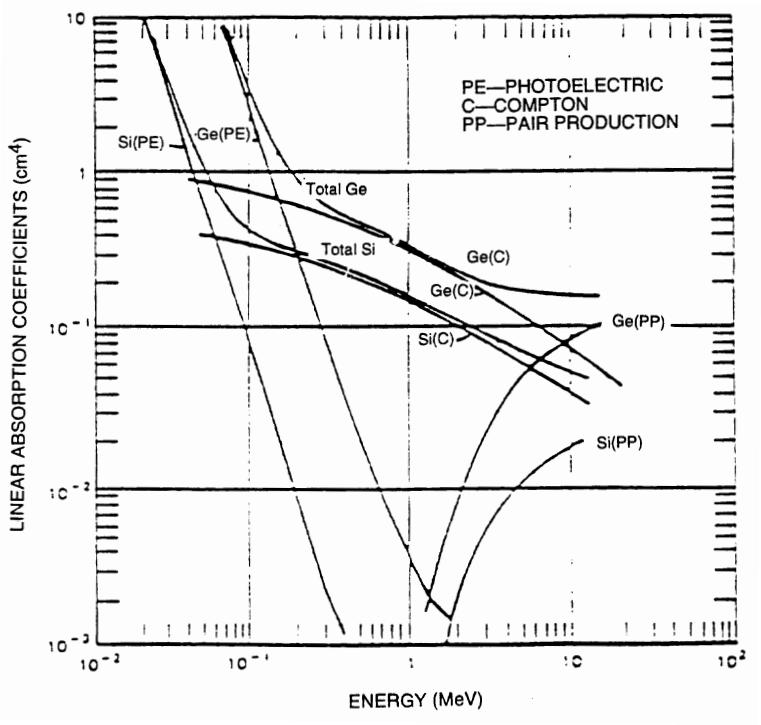

Figure 4-1—Linear absorption coefficients vs. gamma-ray energy for Si and Ge

4.1.4 Average energy ε required for production of electron-hole pairs

In three published studies ([B4], [B12], and[B17][4]), the average energy ε required to produce an electron-hole pair at 77.3 K (the temperature of LN at 760 mmHg) falls into the narrow range of 2.96 to 2.98 eV. However, in each of the studies, the slope of the ε versus temperature curve (at 90 K) is substantially different: –120 ppm /K [B15], –370 ppm/K [B4], and –450 ppm/K [B17]. In the absence of a compelling reason to choose one value over another, the approximate average of the three is used in this standard: 300 ppm/K.

4.1.5 Range-energy relationships in germanium

The thickness of germanium for which there is a 50% probability that a normally incident photon will be absorbed before traversing that thickness is shown in column 2 of Table 4-1. If the photon transfers all of its energy to an electron, the maximum range of that electron is that shown in column 3. There is a wide disparity between the two figures. In practice, the distance of HPGe traversed before all of the photon energy is absorbed, by whatever process, is intermediate between the two extremes. The range-energy relationships are pertinent to the selection of detector geometry for a particular application (see 4.5.1–4.5.3).

Table 4-1—Range-Energy relationships of photons and electrons in HPGe

Energy (keV)	Photon half thickness[a] (mm)	Electron full range (mm)
10	0.05	—
100	8	0.03
1000	21	0.7

[a] The photon half thickness is the range for which there is a 50% probability of photon absorption.

[4]The numbers in brackets correspond to those of the bibliography in Clause 16.

4.1.6 Natural background

Natural background is due to radioactivity in the environment. The background can arise from materials in the cryostat (including the detector element), from radionuclides external to the detector, or from the cosmic-ray continuum. Not much can be done to reduce the background from an existing cryostat, but that from the external environment can be reduced by surrounding the cryostat with a graded shield: a lead outer jacket with a series of liners made of metals with successively lower Z numbers (usually, a lead outer jacket with a single, oxygen-free copper liner is enough).

Typical background spectra obtained with two detectors [B12] are shown in Figure 4-2. The detectors were 55% relative-efficiency p-type HPGe detectors surrounded by a 20 cm low-background lead shield lined with 6 mm of copper;[5] the upper spectrum (A) is from a standard type of cryostat while the lower spectrum (B) is from a detector in a cryostat made from materials selected to have a very low background.

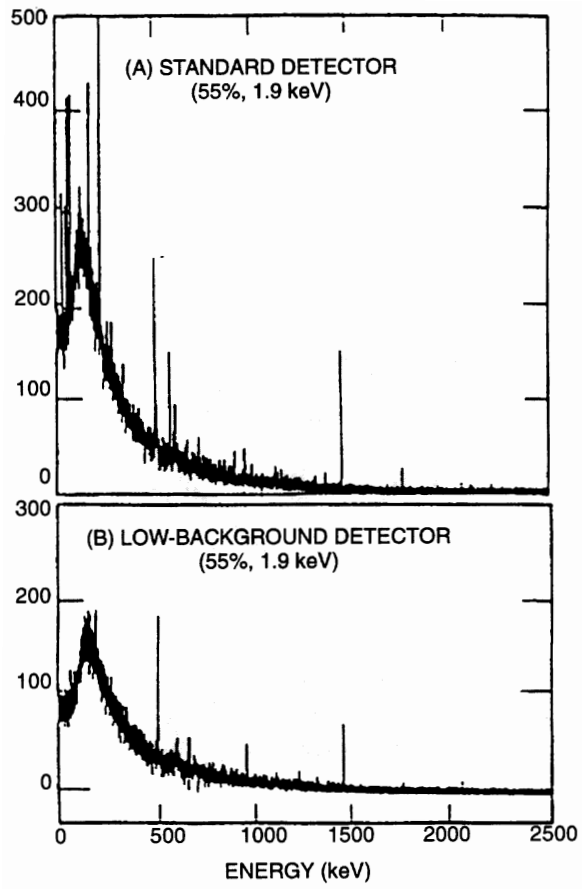

NOTE—Each spectrum was acquired for 100 000 s.

Figure 4-2—Background spectra for two shielded, 55% relative-efficiency detectors (A) Standard cryostat, (B) Low-Background cryostat

[5]This was an experimental shield. Standard practice is to use a copper liner 1.6 cm thick.

4.2 Germanium gamma-ray detector element[6]

A germanium detector element is a diode made by applying suitable electrical contacts to a single crystal of high-purity germanium (HPGe) (IEEE Std 1160-1993). The diode is reverse biased to establish an electric field, causing the detector element to become depleted of free charge carriers. In the depletion region, incoming photons produce a cascade of electron-hole pairs that are swept to the contacts under the influence of the field. The moving charges constitute a current that is proportional to the absorbed photon energy. The current is integrated by a preamplifier to produce an output voltage pulse.

In modern HPGe detectors, the net electrically active impurity concentration (IEEE Std 1160-1993) is typically less than the order of 10^{10} cm^{-3}. As detector elements have become progressively larger, a concomitant reduction in impurity concentration has been required. The high purity is necessary to allow full charge depletion at a reasonable voltage, usually less than 5 kV (see 4.4).

4.2.1 Contacts

The detector element has two electrical contacts (also called electrodes): n-type and p-type, with the n^+ contact biased positively with respect to the p^+ contact. N-type contacts are often made by a lithium diffusion, and p-type by boron ion-implantation, but several other contacting and metallization methods may be used. High-Z metals such as gold are usually avoided because they can produce high-energy fluorescent X rays.

In planar detectors, the contacts are applied to the parallel planes of the disc, one to each plane.

The so-called conventional-electrode coaxial detector is made of p-type germanium with an n^+ lithium contact diffused into the side and bottom of the detector element (outside surfaces) and with a thin, p^+ contact implanted into the sides and bottom of the hole (inside surfaces).

The so-called reverse-electrode coaxial detector is made with a thick n^+ lithium-diffused inner contact and a thin p^+ outer contact. This type of detector has at least two advantages over the conventional-contact one:

a) The thin outer contact extends the detector usability into the X-ray region and makes the detector particularly appropriate for use with anti-Compton shields;
b) Reverse-electrode detectors are more resistant to the effects of fast neutron damage and are also readily restored to their original resolution without a significant loss of efficiency, should such damage occur.

Diffused n^+ contacts are inherently thick: up to 1 mm. In contrast, boron-implanted or metallized (surface barrier) p^+ contacts are usually as thin as 0.3 μm and, by special techniques, can be made as thin as 0.05 μm. Contacts are dead layers because charge carriers formed within them are not collected. The effect is to attenuate radiation passing through a contact, making it desirable to place the thin one at the surface of the crystal through which photons enter. However, it is not always possible to do so, with the result that the usable energy range is above ≈40 keV in detectors with a diffused contact at the entrance. A detector with a 0.05 μm layer can be used down to ≈300 eV.

Detectors damaged by neutron radiation can often be repaired by high-temperature annealing. That process thickens a diffused contact, but not an implanted or metallized one, giving further advantage to detectors with the thin contact at the entrance.

[6]The term *detector* used alone implies the combination of the detector element, cryostat, preamplifier, high-voltage filter, and, in some cases, means of cooling the detector element. The phrase *detector element* is used to denote the germanium crystal with its electrical contacts. In the interest of readability of this standard, the word “element” may be omitted at times when the term is called for, but when such an omission occurs, the intended meaning will be obvious.

4.3 Detector operating and storage temperatures

The germanium detector element is mounted in a cryostat. During operation, it is cooled to a low temperature, typically 80 K to 100 K, which is necessary to reduce leakage current and thermal noise. Cooling is usually by liquid nitrogen (LN), but LN-free, mechanical cooling is an alternative.

The cryostat serves a second purpose: to keep the crystal in an extremely clean environment, which is essential for long-term, trouble-free performance. To enhance the cleanliness, a sorption pump (usually, a molecular sieve) is included in the cryostat to scavenge impurities that may outgas from the internal surfaces.

Although HPGe detectors must be operated cold, they may be stored at room temperature,[7] but there is some risk associated with this practice. When a detector is allowed to warm up, the sorption pump, instead of scavenging gas molecules, gives them off. The crystal is the last item to reach room temperature. During the time that a temperature differential exists between the crystal and its surroundings, gaseous impurities will condense on the surfaces of the crystal. Accordingly, warmup cycles should be completed once begun so that impurities that do condense have an opportunity to evaporate after the warmup is complete. Those impurities will be absorbed by the pump when the detector is next cooled down.

In general, it is desirable not to cycle the cryostat temperature more often than necessary. For example, if a detector is used daily, it should be kept cold continuously rather than be allowed to warm up during the period when it is not in use.

The longer that a cryostat has been kept cold, the greater the amount of gas that will be entrained by the sorption pump. After warmup, the longer the duration at room temperature, the greater the amount of outgassing by the pump and by the interior surfaces of the cryostat. Also, if the detector is kept warm for a period of months, lithium-diffused contacts will grow in thickness. If that type of contact is at the face of the detector, the increased thickness will cause a loss in efficiency when measuring low-energy gamma rays.

Detectors that fall into that category shall be recalibrated when returned to service.

It should be recognized that with the current state of the technology, problems such as those described above may take several years to appear.

4.4 Operating bias and variations in charge collection time

After establishing the bias necessary to fully deplete a detector element, it is usual to overbias it for the following reasons: Above an electric field strength of ≈100 V/mm, electron and hole mobilities ([B15], [B23]) approach a plateau (saturation mobility) of $\approx 10^7$ cm/s. Usually, the bias necessary for full depletion is adequate to establish saturation mobility throughout most of the crystal, but that may not be true in the lowest-field regions. (In a coaxial-geometry detector, the lowest field strength exists at the corner where the face meets the side of the cylinder. See 4.5.2.)

The signal risetime is inversely proportional to the ion mobility. In coincidence measurements, variations in signal risetime are undesirable because they increase the effective resolving time. In amplitude measurements, the *CR* section of the main amplifier's pulse-shaping network is a differentiator, causing the output signal of the shaping network to vary with input-signal risetime. If the risetime varies from pulse to pulse, the energy resolution can suffer because those pulses with longer risetimes produce less signal amplitude, a phenomenon known as ballistic deficit [B7].

[7] In the first germanium detectors (GeLi), electrically active impurity centers were neutralized by lithium atoms diffused into the crystal (lithium compensated), but this practice became obsolete when purer material became available.

The degree to which variations in collection time affect the energy resolution depends on several factors, including the following:

a) The linear dimensions of the detector element relative to the energy of the incoming photons (see 4.1.5). For collection-time variations to matter, the energy must be high enough so that primary photons or those scattered by the Compton process produce electron-hole pairs in the low-field regions of the crystal.
b) The collection time relative to the shaping index of the amplifier. Ballistic deficit is proportional to the square of that ratio [B7]. Usually, when the shaping index is adjusted to minimize the electronic noise, the effect of ballistic deficit is negligible, but this may not be true if both a low-field condition exists in parts of the detector element and the shaping index has been reduced to improve high count-rate performance.

Another justification for overbias relates to the detector-element contacts: In a conventional-electrode coaxial detector (see 4.5.2.1), overbias will cause the depleted region to extend further into the front contact, effectively reducing its thickness. This can improve energy resolution for X rays and low-energy gamma rays.

One of the indicators of nonuniformity of the charge collection time is the ratio of FW.02M to FWHM. For a perfectly shaped Gaussian peak, the ratio is $[(\ln 0.02)/(\ln 0.5)]^{1/2} = 2.38$. If the charge collection time varies from pulse to pulse, tailing is likely to appear on the low-energy side of a peak, causing the ratio to be greater than 2.38.

NOTE—The manufacturer determines the optimum operating bias; it should not be exceeded by the user.

4.5 Detector element classification

Germanium detector elements are classified according to material (n-type or p-type), geometry, and mode of use.

In n-type material, impurities such as As, P, or Sb predominate. These have five valence electrons and therefore produce free electrons (donors). In p-type material, impurities such as Al, B, Ga, or In predominate. These have three valence electrons and therefore produce free holes (acceptors).

The term *geometry* refers to the shape of the detector element and the configuration of electrical contacts. Commonly used geometries are planar and coaxial. Several configurations are shown in Figure 4-3 and described in 4.5.1–4.5.2. Typical planar- and coaxial-geometry detectors with their characteristics are listed in Table 4-2.

For any given application, the choice of the appropriate type and size of detector is a compromise. The factors that must be considered are sample type and size, energy resolution required, the extent to which high-energy peaks from the sample or the natural background generate a Compton background that reduces the ability to resolve low-energy peaks (see 4.1.2), and cost.

All of the preceding factors must be carefully considered. For low-energy measurements, a small detector with low capacitance is often the best choice. For high-energy measurements, a relatively large detector is advantageous (see 4.6).

For a given size of detector, the design is directed towards minimizing the electrical capacitance between the contacts, reducing the thickness of the contact traversed by the photons, increasing the electric field intensity within the unavoidable low-field regions in the crystal (see 4.5.2), and making optimum use of a given volume of germanium. The size is strongly influenced by the need to maximize the peaks of interest while minimizing the Compton background (see 4.1.2). Usually, the larger the detector the higher the efficiency and

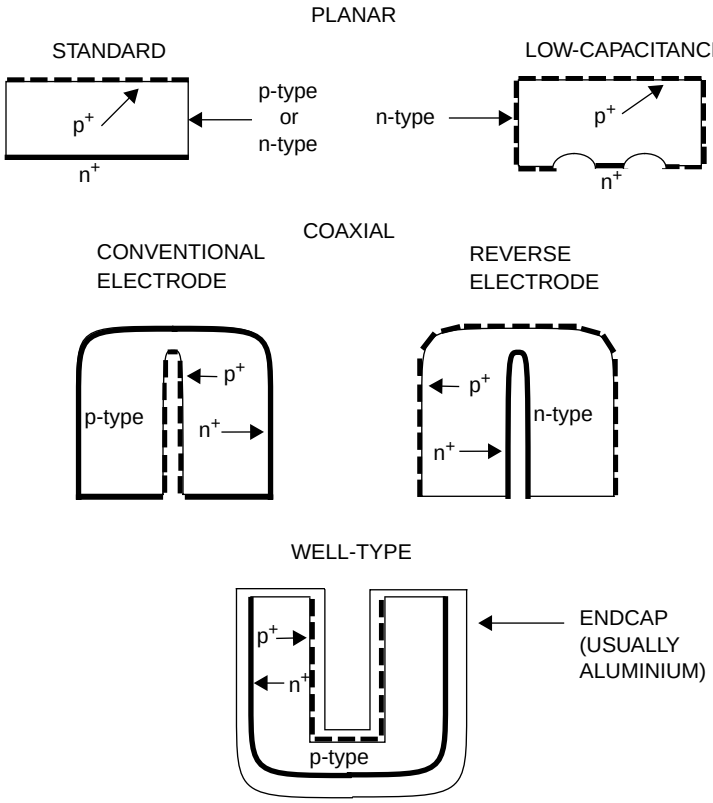

NOTE—Dotted lines represent thin p^+ contacts and heavy solid lines represent relatively thick n^+ contacts.

Figure 4-3—Basic detector element geometries

Table 4-2—Photon detectors and their characteristics

Useful energy range	Geometry	Window thickness	Remarks	FWHM	Peak-to-Compton ratio
3–600 keV	Conventional and modified planar	0.3 μm	3–70 mm diameter	150–700 eV at 5.9 keV 480–900 eV at 122 keV	
0.3–300 keV	Modified planar (ultra-low energy)	0.05 μm	—	120–160 eV at 5.9 keV 480–600 eV at 122 keV	
40 keV–10 MeV	Closed-end coaxial, conventional electrode	300 to 1000 μm	10–160% efficiency[a]	0.7–1.2 keV at 122 keV 1.7–2.3 keV at 1.33 MeV	40:1–110:1
3 keV–10 MeV	Thin-window coaxial, reverse electrode	0.3 μm	10–100% efficiency[a]	0.66–1.2 keV at 5.9 keV 0.7–1.3 keV at 122 keV 1.8–2.5 keV at 1.33 MeV	40:1–90:1
3 keV–1 MeV	Short, thin-window coax, reverse electrode	0.3 μm	36–70 mm diameter	300–500 eV at 5.9 keV 500–700 eV at 122 keV	
10 keV–10 MeV	Coaxial well	0.3 μm	70–500 cc active vol.	1.2–1.5 keV at 122 keV 1.9–2.5 keV at 1.33 MeV	

[a]Relative to a 76 mm × 76 mm (3 in × 3 in) NaI(Tl) scintillation detector.

the higher the peak-to-Compton ratio (P/C).The loss in resolution with a large detector when compared with a smaller one is usually modest.

4.5.1 Planar geometry

A conventional planar geometry detector element is one in which the electrodes (contacts) are parallel planes on opposite sides of a wafer, typically in the form of a circular disc. The p-type electrode is either ion implanted or of the surface-barrier type (metallic layer); the n-type electrode is usually a diffused lithium contact.

Compared with coaxial geometry, discs have a poor ratio of electrical capacitance to volume. For this reason, planar geometry is rarely used for photon detectors larger than 7 cm in diameter by 3 cm deep.

One variation of a planar detector is made with a grooved structure on the back. The grooves reduce leakage current and edge effects. Another variation, called a “modified planar,” is made with a rear contact that occupies only the central portion of the disc and a front contact that overlaps the cylindrical edges. This configuration has a much lower capacitance than the conventional one, resulting in lower noise and better energy resolution, particularly at low energies. Special versions have ultra-thin contacts and are usable down to a few hundred electronvolts.

Because of the volume limitation imposed by the need for low electrical capacitance, planar and modified planar detectors are usually used at the low end of the energy scale.

4.5.2 Coaxial geometry

To maximize the detection efficiency and the peak-to-Compton ratio in the measurement of high-energy gamma rays, a large detector volume is required (see 4.1.2). The electrical capacitance in such a detector is minimized through the use of coaxial geometry.

A coaxial detector element is made in the shape of a right circular cylinder with a coaxial hole (also called a “core”) 8–10 mm in diameter extending from the rear to within 10–15 mm of the front face. The outer electrode covers the front face and sides of the cylinder; the inner electrode covers the surface of the hole (see Figure 4-3). To increase the electric field intensity at the corner where the front face meets the walls of the cylinder, the corner is rounded.

In a rare variation of coaxial geometry, a through hole is used instead of a blind one. In this configuration, the electrodes are applied only to the outer surface of the cylinder and the inner surface of the hole; the corners are not rounded.

Coaxial geometry is practical for detectors with a diameter-to-length ratio not greater than three; most detectors have a ratio of approximately one. Volumes can range from 50 to 700 cm^3. In general, the larger the volume, the higher the counting efficiency and the smaller the ratio of Compton background counts to percent efficiency.

Detector manufacturers shall specify the length and diameter of the detector element and the distance between the front face and the face of the endcap.

The three main varieties of coaxial-geometry detector elements are described in 4.5.2.1–4.5.2.3. Comments on cryostat windows appear in 4.5.3.

4.5.2.1 Conventional-Electrode (standard-electrode) coaxial geometry

The conventional (standard) coaxial detector is made of p-type HPGe, has a lithium-diffused n^+ outer contact ranging in thickness from 0.3 to 1 mm, and a p^+ inner electrode consisting either of implanted boron

ions or of a surface-barrier contact (metallic layer). There are special versions that have a thin enough outer contact to extend the lower limit of energy detection to ≈3 keV. These versions require a cryostat window that minimizes photon attenuation (see 4.5.3).

4.5.2.2 Reverse-Electrode coaxial geometry

A reverse-electrode detector element has the same physical appearance as a conventional-electrode type, but is made of n-type HPGe, has a p^+ ion-implanted outer contact, and an n^+ lithium-diffused inner contact.

The reverse-electrode configuration has two advantages over the conventional-electrode type: a) the thin outer contact extends the usable energy range down to ≈3 keV in contrast with ≈40 keV for the conventional electrode type, and b) reverse-electrode detectors can be more fully repaired after exposure to a damaging amount of neutron irradiation (see 4.2.1).

Special versions with extreme aspect ratios (diameter/length) and shallow holes (to minimize capacitance) are especially suited to low-energy measurements.

4.5.2.3 Well-Type geometry

A well-type detector is a variation of a coaxial detector in which the hole in the detector element is larger than usual. The endcap has a mating well that fits into the hole (see Figure 4-3). The arrangement allows a radioactive sample to be placed close to the center of the crystal. In this location, the sample will be almost completely surrounded by active detector material, greatly increasing the counting efficiency in contrast to placing the same sample outside of the detector.

The crystal well can be a through hole or a blind hole. The latter exhibits higher counting efficiency, particularly for low energies.

Typical endcap openings are 10–18 mm, but may be as large as 25 mm. The hole in the detector element must be ≈4 mm larger than the one in the endcap, and typical depths are 35 to 40 mm. Larger openings are impractical because of the sacrifice in active detector material and an increase in capacitance, which result in a loss of detection efficiency and an increase in noise, respectively. Typical active volumes of the detector element range up to 500 cc. Dimensions are usually set by the needs of the user.

The manufacturer shall give the following:

a) The dimensions of the detector element
b) The dimensions of the endcap well
c) The thickness of the endcap walls
d) The spacing between the facing surfaces of crystal and the endcap well
e) The dimensions of the hole in the crystal

A conventional-geometry detector element is usually used for a well-type detector so that the thinner of the two electrodes is located between the source and the crystal (see 4.2.1).

4.5.3 Endcaps

The endcap covers the detector element and is usually made of aluminum, but is sometimes made of copper or magnesium for low-background applications. For maximum transmission of low-energy photons, a window made of beryllium or other low-density material may be used. Care must be taken in choosing the material to ensure an impermeable window. In many applications the source of the radiation is placed close to the endcap, or it may have a well in it to contain a source for obtaining maximum possible counting efficiency (see 4.5.2.3), or the source may surround the endcap (see 10.6).

4.6 Figure of merit

To date, detectors with relative efficiencies as high as 160% are available and have a marked advantage over smaller ones to the extent that a figure of merit (FoM) has been established ([B12], [B25]). The FoM is useful not only for environmental studies where background limits the minimum detectable activity (see 4.1.2 and 4.1.6), but also for applications such as in-beam nuclear experiments and neutron activation measurements on small samples.

The detector's FoM is obtained from the measured resolution, the peak-to-Compton ratio, and relative efficiency, all at 1.33 MeV:

$$\text{FoM} = \eta_{\text{rel}} \, [(\text{P/C}) \, / \Delta]^{1/2} \tag{4-1}$$

where

FoM is the figure of merit
η_{rel} is the relative efficiency (%)
P/C is the peak-to-Compton ratio
Δ is the resolution (FWHM, keV)

The MDA is inversely proportional to the FoM.

Examples of the MDA at energies from 300 keV to 1 MeV [18] **[BAD REF # IN DRAFT]** are shown in Figure 4-4. Note that the curves in Figure 4-4(A) have similar but not identical shapes at energies from 325 keV to 936 keV. Figure 4-4(B) shows the benefit of the higher P/C in that the background relative to detector efficiency decreases with increasing detector size (see discussion of background in 4.1.2 and 4.1.6).

4.7 Preamplifiers

Preamplifiers fall into two broad categories: voltage sensitive (VSP) and charge sensitive (CSP) (IEEE Std 301-1988).

A VSP exhibits a high-input impedance; for a given charge generated in the detector, the output voltage is inversely proportional to the total capacitance seen at the input of the preamplifier. Because the detector capacitance varies with bias voltage in a detector not fully depleted, a VSP is not used with semiconductor detectors.

CSPs, which are universally used in high-resolution germanium spectrometers, exhibit very low impedance at their input terminals. The signal charge appears across a very stable (25–50 ppm/K), low-noise feedback capacitor, C_{f}, making the output signal virtually independent of the detector capacitance. However, the ratio of the rms series noise signal to the peak signal increases as $C_{\text{t}}^{1/2}$, where C_{t} represents the total input capacitance, making it highly desirable to minimize it.

The packets of charge generated by incoming photons pile up on C_{f}. If not removed, the preamplifier will saturate after a finite number of events. To prevent this, a resistor, R_{f}, can be connected across C_{f} to leak off the charge. The first CSPs were built that way, and many still are, but the resistor contributes noise and does not prevent saturation at very high counting rates (see Clause 7). In other modern preamplifiers, a reset mechanism is used to remove the charge after N events, where N is inversely proportional to the energy of the detected photons. Several types of reset circuit can be used. The details are unimportant for this discussion; what is important is that the reset mechanism eliminates the need for a feedback resistor, resulting in lower electronic noise and a much higher usable counting rate.

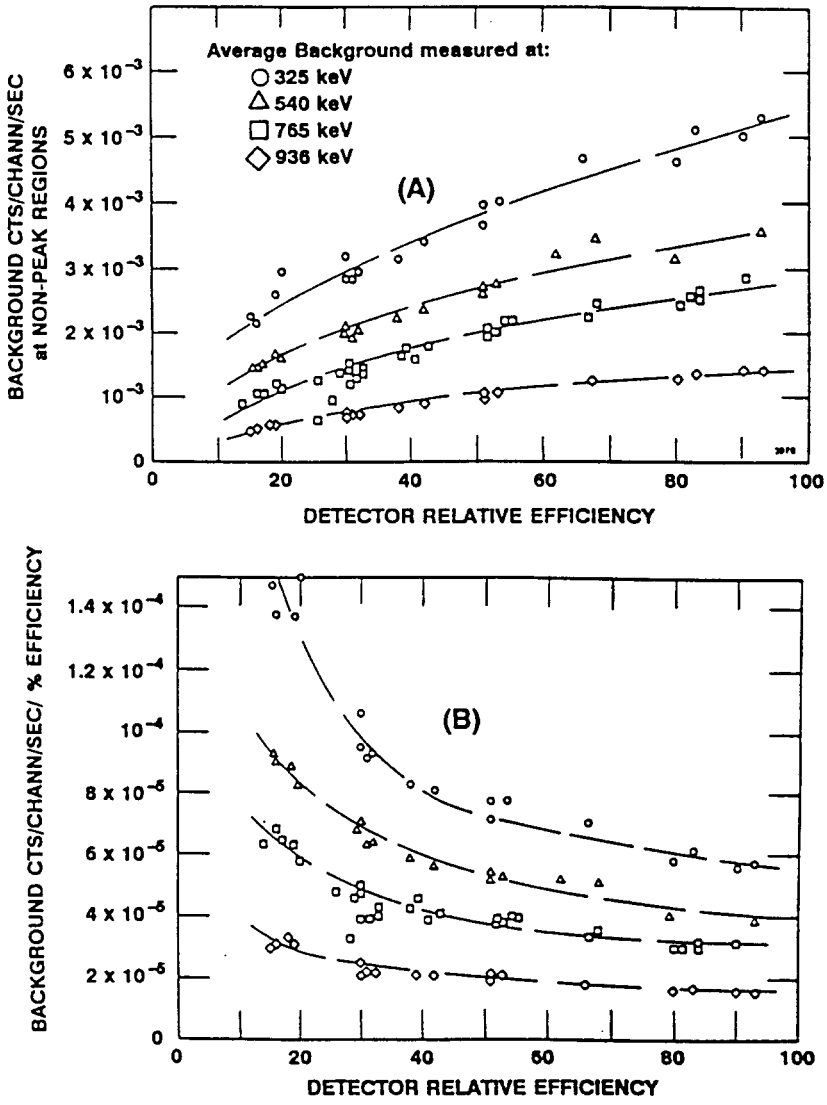

Figure 4-4—Background counting rates in the presence of a mixed $^{152}Eu/^{154}Eu/^{125}Sb$ source vs. detector efficiency

(A) Absolute counts, (B) Counts relative to percent efficiency

5. Detector tests

In a very good HPGe detector, the FWHM is ≈1.65 keV for the 1332.5 keV peak of ^{60}Co. In this standard, the goal for measurement tolerance at that energy is ±20 eV (tolerance of ±1.2%).

5.1 General test requirements

The following shall apply to all tests and measurements described in this standard:

a) To prevent permanent changes of detector characteristics, maximum detector bias, device ambient temperature and environment, and other operational limits specified by the detector manufacturer shall be observed.
b) The detector bias supply, amplifier, multichannel analyzer, and other test equipment shall not have a greater effect on the detector parameter measurements because of instability, nonlinearity, or other performance defects than the stated precision of those measurements. The same shall apply to pickup of internal or external sources of noise.
c) Changes in test system components during a test (for example, an amplifier module) shall not be made without system recalibration. Results affected by the change of more than one parameter shall show explicitly the effects of each parameter change.
d) The values of the measured parameters shall be reproducible within the stated precision of the measurement.
e) The number of significant figures stated shall be consistent with the accuracy or precision of the measurement.

5.2 Test setup for resolution and efficiency measurements

A block diagram of a setup for measuring energy resolution and detector efficiency is shown in Figure 5-1.

A modern multichannel pulse-height analyzer (MCA) typically consists of a small, general-purpose computer with the analog-to-digital converter (ADC) often constructed as a plug-in card. If many lengthy, drift-free runs are to be made, it may be desirable that the ADC be digitally stabilized.

5.3 Temperature sensitivity

Test runs that last for an hour or more may show worse energy resolution than is observed with shorter runs. The likely cause of this is sensitivity of spectrometer components to changes in temperature. To highlight the sensitivity of a modern spectrometer to small changes in calibration, it is instructive to consider the FWHM of the 1332 keV peak of ^{60}Co as a percentage of its energy when measured with a detector exhibiting a FWHM of 1.65 keV: that figure is ≈0.12%. A drift of 0.012% (one channel in ≈8000) will cause a 10% error in the determination of FWHM (165 eV for a 1.65 keV detector). These figures will be used as a benchmark in the material that follows.

Because of the thermal mass of the system, a sudden change in ambient temperature may take an hour or more to affect performance.

5.3.1 Electronic system

The components most likely to be affected by temperature changes (ΔT) are the gain and dc zero of the main amplifier, the conversion gain and zero intercept of the ADC, and the detector element.

The gain of the amplifier and ADC can be made temperature stable to 0.002%/°C (20 ppm/°C) or less, and the dc zero to 10 μV/°C (0.01 channels in an 8000 channel ADC). Using the benchmark figure stated above,

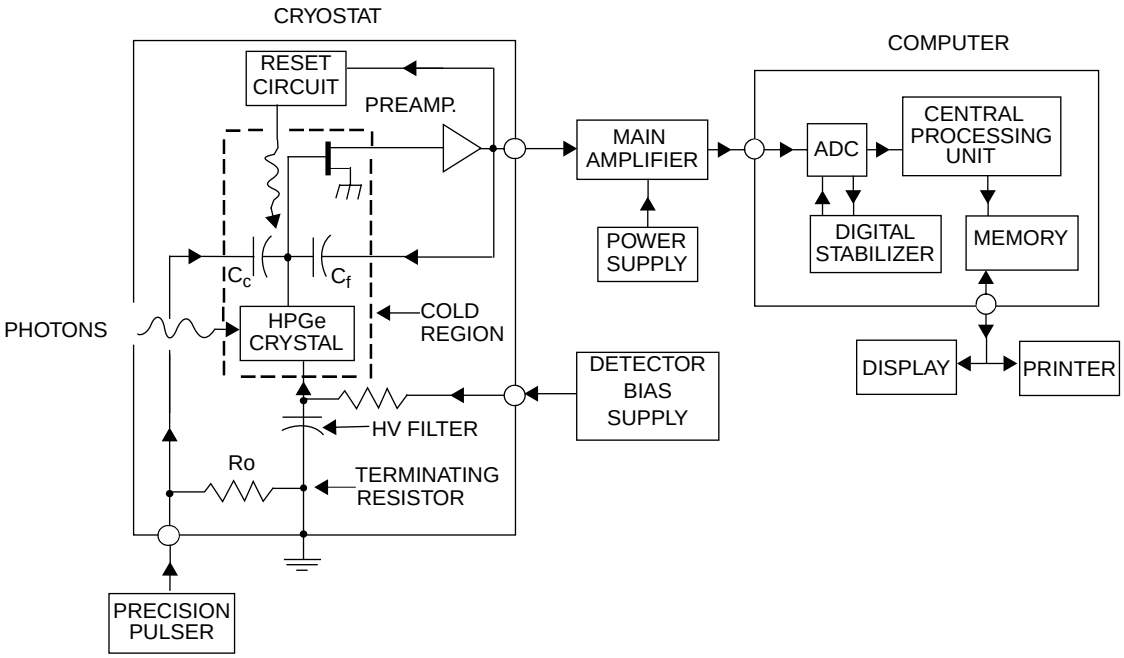

Figure 5-1—Block diagram of a typical germanium gamma-ray spectrometer

a ΔT of 6.5 °C would produce a gain shift of 0.013% (130 ppm) and the negligible zero shift of 0.065 channels. However, this stability depends on the combined stability of many separate components in the electronic chain, any one of which can become faulty.

5.3.2 Detector element

A liquid nitrogen bath insulates the detector element from changes in room temperature, but not from changes in atmospheric pressure. Changes in the latter affect the boiling point of LN, therefore the crystal temperature and the value of ε (see 4.1.4). Pertinent formulas are given in 5.3.3–5.3.6, from which it will be seen that only in rare circumstances must corrections be made. For example, a change in altitude of 1 km (≈4700 ft) causes a change in ε of only 0.03%.

It should be noted that a mechanical cooler does not have the temperature stability of a liquid nitrogen bath.

5.3.3 Liquid nitrogen temperature vs. pressure

It can be shown that the boiling point of LN and the atmospheric pressure are related by [B26], p. 6-92:

$$T = 39.84\, P^{0.1} \text{ or} \tag{5-1}$$

$$P = (T/39.84)^{10} \tag{5-2}$$

where

T is the temperature (K)
P is the pressure (mmHg)

The error is < ±0.5% from 300 to 1000 mmHg.

5.3.4 Atmospheric pressure vs. altitude

From sea level to 10 km (0 to 33000 ft), the atmosphere pressure changes with altitude[8] according to

$$P = 760 \exp(-0.125H) \quad (5\text{-}3)$$

where

P is the pressure (mmHg)
H is the altitude (km)

5.3.5 Liquid nitrogen temperature vs. altitude

From Equations 5-1 to 5-3 and Subclause 5.3.4, the temperature of LN vs. altitude varies according to

$$T = 77.34 \exp(-0.0125H) \quad (5\text{-}4)$$

where

T is the temperature (K)
H is the altitude (km)

5.3.6 Change in ε at 90 K versus atmospheric pressure

From Equation 5-1 and the tempco of ε of –300 ppm/K (Subclause 4.1.4), ε changes by +3.1 ppm per mmHg (+0.1 ppm per inHg) at 90 K.

For weather to produce the benchmark change of 130 ppm (Subclause 5.3.1), the barometer would have to change by 130/3.1 = 43 mmHg (1.43 inHg). This can occur during an extreme weather change, but is unlikely to occur during a test run.

From Equation 5-4, changing the altitude of the detector will change the energy calibration by +290 ppm per km of altitude (61 ppm per 1000 ft). This is a change of only 0.38 keV per km of altitude in the 1332.5 keV line of ^{60}Co (0.08 keV per thousand feet).

5.4 Amplifier pulse shaping

Modern linear (non-gated) pulse-shaping networks are based on a differentiating section (*CR* section) followed by six integrating sections (*RC* sections) having varying time constants that bear a particular relationship to the *CR* section. Depending on the pattern, the waveforms are quasi-Gaussian or quasi-triangular (see IEEE Std 301-1988, [B7], and [B10]) with the most popular of the quasi-Gaussian networks being the "sine^n network" that produces a waveform expressed by $v(t) = V_p \exp(-3t) \sin^n t$. A comparison of the two networks shows that for a given width at the 50% pulse-height level ($t_{0.5}$), the quasi-triangular (Q-T) [B10] waveform is narrower than the sine^n waveform when measured near the baseline (at 1% of peak height, or $t_{.01}$), giving the Q-T network a 9% resolving-time advantage. The Q-T network also has a slight noise advantage of 0.3%.

To improve the noise performance and/or the resolving time beyond that possible with linear shaping networks, gated integrators must be used ([B18], [B19]).

[8]Equation 5-3 is based on data obtained from an office of the National Oceanic and Atmospheric Administration, U.S. Department of Commerce. The pressure figures were not corrected for temperature. At sea level, the temperature was 290 K; at 5 km, it was 256 K, but the departure of Equation 5-3 from the data is < 1%; at 10 km, the figures are 198 K and 10%, respectively.

When stating detector performance, the type of shaping shall be given (quasi-Gaussian, quasi-triangular, or gated integrator) and, when linear shaping networks are used, the shaping index $t_{0.5}$ and resolving time $t_{.01}$ shall be specified.

5.5 Electromagnetic interference

Electromagnetic interference from external and internal sources of noise can adversely affect the evaluation of a spectrometer. If certain rules are followed in the interconnection of the test instruments, it is usually possible to eliminate the interference.

Examples of external noise generators are local radio stations, fluorescent lights, and nearby computers. Examples of internal noise generators are modular instruments containing switching power supplies and the instrument bin itself (NIM bin; see DOE Report DOE/ER-0457T). Detectors with special shields to block the direct pickup of electromagnetic radiation have been built, but unless careful attention is paid to the interconnections of the various components of a spectrometer, it is still possible for external noise to find its way into a system.

Extraneous noise shall be reduced to a level that does not affect the measurement of system parameters by more than the accuracy stated by the manufacturer. The noise sources and how to cope with them are described below.

5.5.1 Noise pickup from ground loops

A typical instrument setup for measuring the resolution and efficiency of a detector is shown in Figure 5-1. If the separate components of the measuring system are improperly configured, ground loops will be set up that provide points of entry for unwanted signals.

An example of a ground loop is the combination of a test-pulse generator and a spectrometry system in which the generator is plugged into one wall outlet (power outlet) while the remainder of the system is plugged into a different one. The loop is completed through the coaxial cable that joins the output of the generator to the test-input receptacle of the preamplifier, and a second loop is set up when the direct output of the generator is connected to the external trigger input terminal of the oscilloscope.

Transient ground currents can be caused by electrical equipment in the building. If those currents pass along the power line between the two wall outlets, an interfering signal will be introduced into the loop. If the cables and line cords are long and spread out, the loops make effective antennas for the pickup of interfering electromagnetic radiation. The larger the area bounded by the loops, the more effective the antenna.

The induced noise currents depend on the magnitude and frequency of the interfering radiation and on the impedance of the loop (its inductance and resistance). It might be argued that these circulating currents do not matter because of the shielding inherent in the coaxial cables connecting various parts of the system, but the circulating currents *do* matter: aging connectors exhibit increasing electrical resistance at their mating surfaces, allowing a voltage drop to appear in series with signal path. The same is true of the voltage drop from one end of a signal cable to the other because of its non-zero impedance. Finally, the outer shield of a flexible cable is made of woven braid that inevitably has gaps between the individual wires. The gaps permit coupling of the ground-loop current into the center conductor; the one carrying the desired signal. The interfering signals can be comparable in size to the ones generated in the detector, particularly in the X-ray range.

Another frequently overlooked characteristic of typical bins is that line-frequency voltage of the order of 10 mV may exist between the front and rear and between the lateral ends of the bin. This voltage arises because the bin acts as a one-turn loop into which the stray magnetic field of the bin's power transformer induces a current. To break this ground loop in amplifiers that have input and output signal connectors duplicated on front and rear panels, manufacturers insulate the connector shells from the panels.

5.5.2 Examination for noise pickup from ground-loops and from other sources of external noise

Both an oscilloscope and an MCA are necessary to find extraneous sources of noise. Each must be used to check the other because each may be its own source of noise.

The following procedure will help to uncover noise injected into the system from parasitic noise generators:

a) The oscilloscope (dc-coupled) shall be connected to the output of the main amplifier. Radioactive sources shall be removed from the detector.
b) If possible, the baseline restorer (BLR) in the amplifier shall be deactivated to keep it from masking low-level noise.
c) With the oscilloscope trigger sensitivity set high (internal triggering), the oscilloscope signal-channel sensitivity shall be increased so that shaping-amplifier noise (“grass”) is clearly visible. Then, the trigger sensitivity shall be reduced so that it triggers only on the noise peaks. (Because of the statistical nature of random noise, the initial noise peak will always appear ≈2.4 times larger than the average noise level. This initial peak should not be interpreted as being due to external-noise pickup.)
d) The sweep speed shall be switched slowly through the range of 10 ms/DIV to 50 ns/DIV (a DIV is a main graticule division) while looking for patterns of repetitive noise on the oscilloscope screen.
e) The last step shall be repeated with the trigger set for line-frequency triggering.
f) The procedure shall be repeated with the MCA connected and disconnected, with it accumulating counts and with it quiescent, with a test-pulse generator connected and disconnected (but with the generator quiescent), and with the direct-output terminal of the generator connected and disconnected from the trigger input receptacle of the oscilloscope.
g) If a repetitive noise pattern appears, the detector bias shall be changed (or switched off) to determine whether the bias supply is the source of noise.
h) Any patterns that show up shall be correlated with phantom lines or line broadening that may appear in a recorded spectrum.
i) Finally, the spectrum shall be examined for changes that may be caused by connecting and disconnecting the oscilloscope from the system.

Removing the radioactive sources from the detector (step a) will not reduce the counting rate to zero because there is always some background radiation present. The background pulses will saturate the oscilloscope. With most oscilloscopes, those pulses interfere seriously with the examination of noise-level signals. That problem can be reduced or eliminated by connecting a pulse-clipping fixture between the output of the main amplifier and the input of the oscilloscope (see Figure 5-2). This fixture will limit pulse heights seen by the oscilloscope to ≈1 V; the amplifier gain must be adjusted so that the height of the random-noise envelope is ≤200 mV.

A carefully configured spectrometer should show no external noise pickup, but achieving that ideal may be difficult—eliminating ground-loop noise can be a lengthy trial-and-error process.

5.5.3 Reduction of noise pickup due to ground loops

Based on the preceding, the two main approaches to lowering external-noise pickup are to reduce the antenna effect by shrinking the area enclosed by the cables and line cords, and to increase the inductance of the ground loop without increasing the area it encloses, thereby decreasing the magnitude of the circulating current. The following guide lines shall be followed in setting up a spectrometer:

a) All power cords, including the one from the monitoring oscilloscope, shall be plugged into one power outlet, using a local power strip to accomplish this.

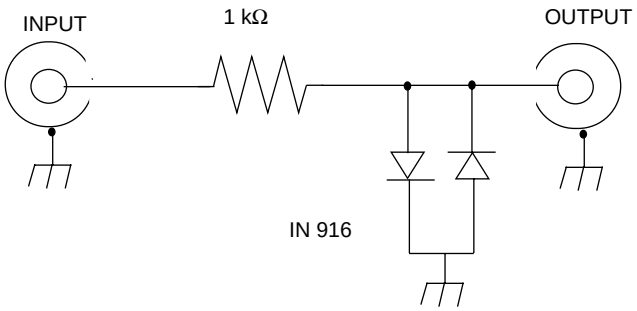

Figure 5-2—Clipping network

b) If possible, all cables connecting the detector assembly to the remainder of the spectrometer shall be made the same length. If this is not feasible, the longer cables shall be folded back on themselves. The individual cables shall be bundled by twisting them together or by binding them with string or tape.
c) If possible, the output cables from the preamplifier and test-pulse generator shall both be connected to the front panel or both to the rear panel of the main amplifier, but not one to each. If the amplifier configuration does not permit this and if connecting the test-pulse generator increases the system noise, step d) shall be tried.
d) As a means of increasing the impedance of the ground loop, the power cord or the output cable(s) of the test-pulse generator shall be threaded through a large ferrite core, making three or more turns (the effectiveness increases as the square of the number of turns). Split cores (rectangular in shape) held together with a thin plastic frame are available for this purpose from one of the retail electronic-parts outlets.[9]
e) The shortest possible connecting cables shall be used between the spectrometer and instruments external to it (MCA, test-pulse generator, oscilloscope).
f) In instrument bins, “quiet” modules shall be inserted between the main amplifier and the “noisy” ones. Modules containing switching circuits such as a switching-regulator power supply or a scaler may be particularly noisy.
g) In stubbornly noisy systems, the enclosures of the various parts of the spectrometer can be joined with large-gauge wire or shielding braid. An external ground connection may help, but the connection shall be made at only one point in the system to avoid setting up another loop.

The use of doubly shielded coaxial cables for the interconnections may also help because the double shielding reduces coupling of ground-loop noise into the center conductor by a factor of 10. Preamplifier/amplifier combinations with balanced-line interconnections can reduce external noise by an additional factor of 10.

[9]One type of these is available from Radio Shack, Catalog No. 273-104.

6. Energy resolution measurements

This clause contains background material for energy resolution measurements. The actual test procedures and the computations that shall be made with the data given in Clause 7.

6.1 Introduction

Modern pulse-height analysis systems include programs for determining FWHM. Some also contain programs for calculating FW.1M and FW.02M, but the algorithms and the accuracy of the results differ among manufacturers. When detector performance specifications are based on the use of an untried MCA, those internal algorithms shall be tested according to the procedures given in this standard.

The simplest built-in algorithms find peak height and peak center by quadratic interpolation and FWHM by linear interpolation. Background subtraction may or may not be included in the program. A more complex algorithm is based on the least-squares fit of a Gaussian distribution to the measured peak, but this may produce errors if the detector exhibits asymmetry in the FW.1M and FW.02M regions.

A spectrum peak displayed on the readout of an MCA usually consists of a group of dots that outline the peak (see 7.2 and Figure 7-1).

Resolution measurements require interpolation between dots. If done visually, the accuracy is subject to the judgement of the observer. In this standard, determination of the peak widths at the 0.5, 0.1, and 0.02 peak-height levels depends on applying formulas to the appropriate channel addresses and counts per channel that are recorded by the MCA. Quadratic interpolation is used for finding the peak height and the peak center, and linear interpolation is used for finding FWHM, FW.1M, and FW.02M. Background and channel-width corrections are included. The formulas presented here can be solved with a programmable pocket calculator.

The calculations described here are not intended to supplant built-in MCA programs unless there is a systematic discrepancy between the figures given by the MCA and those obtained by applying the methods described in this standard (see 6.2.3).

6.2 Resolution specifications and other requirements

Required specifications and test-source requirements are listed below in the following subclauses.

6.2.1 FWHM, FW.1M, and FW.02M

The FWHM, FW.1M, and FW.02M shall be specified, including the limit of error.

6.2.2 Skewing factors

Charge that originates in low electric-field regions of a detector element exhibits a longer collection time than charge from normal-field regions, causing some signal attenuation when passing through an amplifier's linear pulse-shaping network (gated-integrator pulse processing is less subject to this form of attenuation). Also, Compton scattering causes signal losses in some pulses. These show up as an increase of the FW.1M and FW.02M relative to the FWHM. Skewing factors can be defined that give a measure of the effect. In a perfect Gaussian distribution, the ratio of the FW.1M to the FWHM = 1.82, and the ratio of FW.02M to FWHM = 2.38. Thus, skewing factors can be defined as $S_{0.1}$ = FW.1M/(1.82 FWHM) and $S_{.02}$ = FW.02M/(2.38 FWHM). If the peak is perfectly Gaussian, the skewing factors = 1.00; if it is not, they are greater than 1.

The manufacturer shall specify $S_{0.1}$ and $S_{.02}$ for the upper peak of ^{60}Co for detectors that are intended to be used at energies of 1 MeV and above.

6.2.3 Discrepancies

If there are systematic discrepancies between the FWHM figures given by the MCA and those obtained by applying the methods described in this standard, this standard shall prevail.

6.2.4 External electrical noise

Prior to making any tests, the system shall be purged of external electrical noise (see 5.5 through 5.5.3).

6.2.5 Test sources

The spectral peak commonly used for testing energy resolution of a detector is the 1332.5 keV line of the ^{60}Co doublet. At this energy, the resolution should be dominated by detector characteristics rather than by electronic noise. At lower energies, such as at the energies of the ^{57}Co 122.1 and 136.5 keV lines, electronic noise contributes significantly to the resolution.[10] In the interest of standardization, it is desirable that everyone use the same radionuclides for resolution tests. Recommended sources for calibrating and testing a spectrometer are given in Table 6-1.

Table 6-1—Radionuclides for energy resolution and other measurements

Radionuclide	Half-Life	Energy
^{55}Fe	2.74 years	5.90 keV[a]
^{241}Am	433 years	59.54 keV[a] and 26.3 keV X rays
^{109}Cd	463 days	22.2 keV[a] and 88.0 keV[a] (X-ray doublet)
^{57}Co	272 days	122.1 keV[a] and 136.5 keV
^{137}Cs	30.2 years	661.7 keV[ab]
^{22}Na	2.60 years	1274.5 keV[a]
^{60}Co	5.27 years	1173.2 keV and 1332.5 keV[ac]
^{208}Tl	1.91 years	2614.5 keV[a] (^{228}Th source)

[a]Gamma and X rays recommended for energy resolution measurements.
[b]Short-Lived X rays with energies of 31.8, 32.2, and 36.4 keV are produced by the ^{56}Ba daughter.
[c]This line is preferred for coaxial detector specifications.

6.2.6 Point source

A standard source is usually prepared in the form of a disc upon which the radionuclide is deposited in solid form, usually by evaporation from solution.

Discs made of high-Z materials (metals) should be avoided because of Compton effects. In this standard, a point source is defined as a disc in which the diameter of the active region of the radionuclide is ≤ 2 mm. (The thickness of the active material is essentially zero; an active region 2 mm in diameter is so small that the solid angle of the photons intercepted by the detector element is nearly independent of where in the source the photons originate.)

[10]A useful (but dimensionally incorrect) empirical formula for energy resolution in an HPGe detector is $R = [(\Delta E_E)^2 + 2E]^{1/2}$, where R is the FWHM at energy E and ΔE_E is the noise line width (FWHM), with all terms in units of electronvolts.

6.2.7 Source placement, standard coaxial detector

A point source shall be

a) Located axially with respect to the detector element
b) 25 cm from its face
c) With the plane of the source parallel to the face of the detector element
d) With nothing but air between the source and the detector assembly

High-Z objects (shields, supports, etc.) in the vicinity of the setup can scatter photons into the detector element. Those objects shall be small enough or far enough away so that the photons scattered into the detector amount to ≤2% of the direct beam from the source.

The manufacturer shall give the distance between the window of the cryostat and the facing surface of the detector element.

6.2.8 Source placement, well-type detector

Because some detectors may have poor charge collection near the inner contact as a result of low electric field strength in that region, the primary resolution specification shall be obtained with a point source (see 6.2.6) located on the axis of symmetry, inside the endcap well, and 1.0 cm from the bottom. The nuclides used and the methods of measurement shall be the same as for other configurations.

Note that a detector with a low electric field strength at the inner contact will perform poorly with the source inside the well (particularly the FW.02M performance). Also, the resolution compared with that of a standard coaxial detector having the same efficiency can be expected to be slightly worse because the relatively large hole necessary for well-type geometry increases the electrical capacitance, thereby degrading the signal-to-noise ratio. In a coaxial or well-type detector, the capacitance varies approximately as the logarithm of the ratio of the hole diameter to the outer diameter.

A well-type detector can be used with the test source external to the well; the counting efficiency and peak-to-Compton ratio will suffer, but the energy resolution may improve. For those who intend to use the detector in such situations, it is recommended that the manufacturer specify performance for both external and internal sources, clearly indicating the source placement with respect to the cryostat's axis of symmetry.

6.2.9 Channel-Width calibration

For the measurement of resolution, the system shall be calibrated in electronvolts or kiloelectronvolts per channel (see 7.5.5). Two peaks shall be used for this purpose, with energies close enough to the peak under study to avoid errors due to system nonlinearities. In the vicinity of 1 MeV, the 1173.2 and 1332.5 keV lines of ^{60}Co shall be used. In the region near 100 keV, the 122.1 keV and 136.5 keV lines from ^{57}Co shall be used. If the resolution test is made with a monoenergetic gamma emitter, it will be necessary to use an additional source to provide the second peak. A pulse generator can be used for this purpose, but its pulse height dial must contain at least as many fine divisions as there are channels in the ADC, and the differential nonlinearity of the pulse-height setting must be better than that of the ADC.

6.2.10 Counting rate

As the counting rate increases from zero, random overlap between successive pulses increases, a phenomenon known as pulse pile-up. The effect is to cause peak broadening by skewing the peak towards the high-energy side. The counting rate referred to here is that of all events above the system noise level, not just the counting rate of the test peak.

The permissible counting rate is inversely proportional to the amplifier shaping index and shall be arrived at by starting at a rate greater than 10 000 counts per second (c/s), then reducing it in increments while graphing the resolution vs. the rate. It will be observed that a plateau is approached as the rate is reduced. An acceptable rate, and the one at which resolution tests shall made, is the one where any further reduction does not improve the resolution by an amount more than the acceptable error band of the measurement. At that counting rate, the product $nt_{0.5}$ shall be recorded, where n is the rate in c/s and $t_{0.5}$ is the shaping index[11] in μs. The figure shall be furnished as part of the specifications of the detector. (The figure $nt_{0.5}$ is usually of the order of 10 000, but may depend on the shape of the spectrum and the isotope used.)

6.2.11 Total noise line-width and detector contribution

Contributions to peak broadening in a spectrometer are the variance in the number of hole-electron pairs produced by monoenergetic gamma rays,[12] electronic noise, and variations in collection time from different parts of the detector.

The noise components due to the preamplifier are the equivalent series resistance of the input transistor, $1/f$ noise in that transistor, shunt resistance of the feedback resistor (if one is used), and dielectric losses in insulating materials ([B7], [B9], and [B18]). The resolution is also degraded by capacitance across the input terminals of the preamplifier, which is made up of the detector capacitance, input capacitance of the preamplifier, and the capacitance of the electrical connections of the detector element to the preamplifier. This capacitance does not generate noise, but it attenuates the signal[13] while leaving the noise unaffected, thereby degrading the signal-to-noise ratio.

In principle, the electronic noise can be measured with a wideband ac voltmeter if the detector is replaced by a capacitor (IEEE Std 300-1988), but this is impractical in a modern system because the detector element and input transistor of the preamplifier are sealed within the cryostat. If an ac voltmeter is connected to a working system, pulses caused by background radiation from the environment will overload the voltmeter and interfere with the measurement. This problem can be reduced by interposing a pulse-height limiting network between the pulse amplifier and the voltmeter, but unavoidable errors still occur.

If the system contains a pulse-reset preamplifier, the reset pulses produce even more interference than the background radiation.

Finally, even if the preceding problems can be bypassed, the ac voltmeter will give a correct indication only if the baseline restorer in the main amplifier is deactivated. This cannot be done in some modern amplifiers.

The only practical means of measuring the electronic noise is by using a pulse generator to simulate a photon pulse from the detector (see subclauses 7.3 and 7.3.1). The FWHM of the generator peak is equivalent to the FWHM of the electronic noise contribution to the system. By applying Equation 6-1, that contribution can then be quadratically subtracted from the measured total resolution to give the resolution ΔE_O due primarily to the charge generation and collection processes in the detector.

$$\Delta E_O = \sqrt{(\Delta E_S)^2 - (\Delta E_T)^2} \tag{6-1}$$

where

[11] $t_{0.5}$ is the width of the amplifier output pulse measured at 50% of its peak height (IEEE Std 300-1988).

[12] Because of correlation effects in the generation of hole-electron pairs (Fano factor), the resolution is better than obtained from calculations based solely on the variance.

[13] Because of the feedback action in a CSP, increasing the input capacitance increases the observed noise level without materially affecting the observed signal height. It can be shown that this occurs because the voltage gain of a CSP (not to be confused with charge "gain") is numerically equal to C_t/C_f, where C_t refers to the total input capacitance and C_f to the feedback capacitance. The increase in voltage gain exactly cancels the reduction in signal voltage Q/C_t, where Q is the charge generated in the detector by a gamma ray.

ΔE_O is the FWHM due to all factors other than electronic noise (keV)

ΔE_T is the FWHM of the pulser peak (keV)

ΔE_S is the FWHM of the measured gamma-ray peak (keV)

6.2.12 Counts in the peak

In using the formulas of this standard to determine the FWHM specification, at least 10 000 counts and preferably 20 000 shall be accumulated in the center channel of the photopeak. If system drift[14] during the counting interval does not permit this, several shorter test runs shall be made such that the sum of the counts in the separate runs adds up to 10 000 or more; the FWHMs computed for those runs shall be averaged.

It may be possible to accumulate fewer than 10 000 (20 000) counts with the built-in programs of the MCA and still fall within the error limit quoted by the manufacturer, but that possibility shall be examined by running a series of tests and evaluating the variations in resolution.

6.2.13 Number of channels across the FWHM

A state-of-the-art detector will exhibit an FWHM of ≈1.65 keV for the 1332.5 keV peak of ^{60}Co. At least five channels shall be included in the FWHM. With an 8192 channel ADC, the channel number in which that peak appears for 5 to 10 channels across the FWHM is given in Table 6-2.

Table 6-2—Kiloelectronvolt per channel *and* address of the center channel vs. channels across the FWHM for the 1332.5 keV ^{60}Co line at 1.65 keV FWHM

Channels across FWHM	keV per channel	Peak-Channel address
5	0.3300	4037.9
6	0.2750	4845.5
7	0.2357	5653.0
10	0.1650	8075.8

The preferred number of channels across the FWHM is 10, but 5-channel peaks require only half the counting time for a given number of counts in the peak channel. If 5-channel peaks are used, errors arise because of the finite width of the channels (see 7.4.4).

6.3 Errors in determining resolution

Errors arise from interpolation between channel addresses, from the finite width of channels, and from statistical fluctuations in the channel counts.

6.3.1 Interpolation errors

With linear interpolation, chords replace segments of the Gaussian curve (see 7.2 and Figure 7-1). Because the chords are not tangent to the curve at the intersections with the resolution lines, an FWHM error of 0.8%

[14] An indication of drift between test runs is a change in the symmetry of the dot pattern that traces out the peak.

can occur (assuming a perfectly shaped, 5-channel Gaussian peak). The 0.8% is relatively low because there is little curvature at the 50% peak-height level. However, at the FW.1M and FW.02M levels, the errors can be 2.2% and 2.4%, respectively, depending on the distribution of the dots that outline the photopeak.

There are no correction formulas for this form of error, but the error diminishes inversely as the square of the number of channels across the FWHM.

6.3.2 Channel-Width error

A channel count indicated by the MCA is proportional to the channel area; that count should indicate the height of the channel at its center, but that number is different from the true height of a Gaussian distribution measured at that location. The difference is an error that is inversely proportional to the square of the number of channels across the FWHM. With a truly Gaussian 5-channel peak, depending on the distribution of the channels with respect to the peak centerline, the apparent FWHM, FW.1M, and FW.02M can be too large by ≈0.8%, ≈2.0%, and ≈2.4%, respectively. This form of error can be reduced to ≈0.1% by a correction formula (see 7.4.4), but it does not reduce the interpolation error described in the preceding subclause.

6.3.3 Errors due to statistical fluctuations

Statistical fluctuations in channel counts are reflected in fluctuations of the measured resolution. The resolution term most affected is the FWHM, and the channel having the greatest effect on the FWHM is the center channel. For example, in a 5-channel peak with $\hat{N}$ = 10 000 counts, a fluctuation of 1% (one standard deviation, or 1σ) will produce a change of 0.7% in the FWHM. The changes in FW.1M and FW.02M will be 0.1% and 0.2%, respectively.

Fluctuations of 1σ in the channel counts containing one of the resolution levels produce at most a 0.2% change in that resolution (but only in a truly Gaussian distribution).

7. Test procedures and computations

7.1 Recording a spectrum

Based on the use of a ^{60}Co test source, a spectrum shall be recorded according to the procedures given in 7.1.1–7.1.3. The data so obtained shall be used for the computations described in 7.4–7.4.7. Corrections may be necessary for peaks in the background (7.1.1) or for a uniformly distributed background (7.4.1).

7.1.1 Background peaks

If a background peak is present and is close enough in energy to overlap a test peak, the background spectrum shall be subtracted from the test-source spectrum. To do this, two measurements are required:

a) A spectrum of the ^{60}Co test source plus background shall be obtained, with at least 10 000 counts in the peak channel of the 1332.5 keV ^{60}Co line. The spectrum and the live time of the measurement shall be recorded.
b) The test source shall be removed and the measurement repeated *for the same live time* as recorded in step a). (The spectrum so obtained is of background alone.)

To make the correction, the counts obtained in step b) shall be subtracted, channel by corresponding channel, from those in step a).[15]

[15]Many MCAs include a built-in routine for subtracting one spectrum from another.

7.1.2 Peak location, test source

With an 8192-channel ADC, a ^{60}Co source, and a 1.65 keV detector, the 1332.5 keV line may be placed in Channel 4032 to obtain five channels across the FWHM (see 6.2.12), or in a lower channel number (see Table 6-2) for a detector with worse resolution.

Test sources other than ^{60}Co may be used (see 6.2.5), but the location of the peaks shall then be modified to meet the requirement of five channels or more being included across the FWHM.

7.1.3 Peak location, pulse generator

When a pulse generator is used for a noise-resolution test with a ^{60}Co test source, the generator peak shall be placed between the two photopeaks. At this location, the width of the generator line will be very narrow. To obtain enough channels across it, the spectrum shall be positioned as close as possible to the top of the ADC range. (The resolution and energy calibration tests can be made with the spectrum in this location instead of the one described in 7.1.2, but it may be more convenient to separate the noise-resolution test from the preceding ones.)

7.2 Sample spectrum, 1332.5 photopeak of ^{60}Co

A sample spectrum of the 1332.5 keV peak of a ^{60}Co source,[16] plotted to a linear scale, is shown in Figure 7-1. The counts vs. channel number appear in Table 7-1.

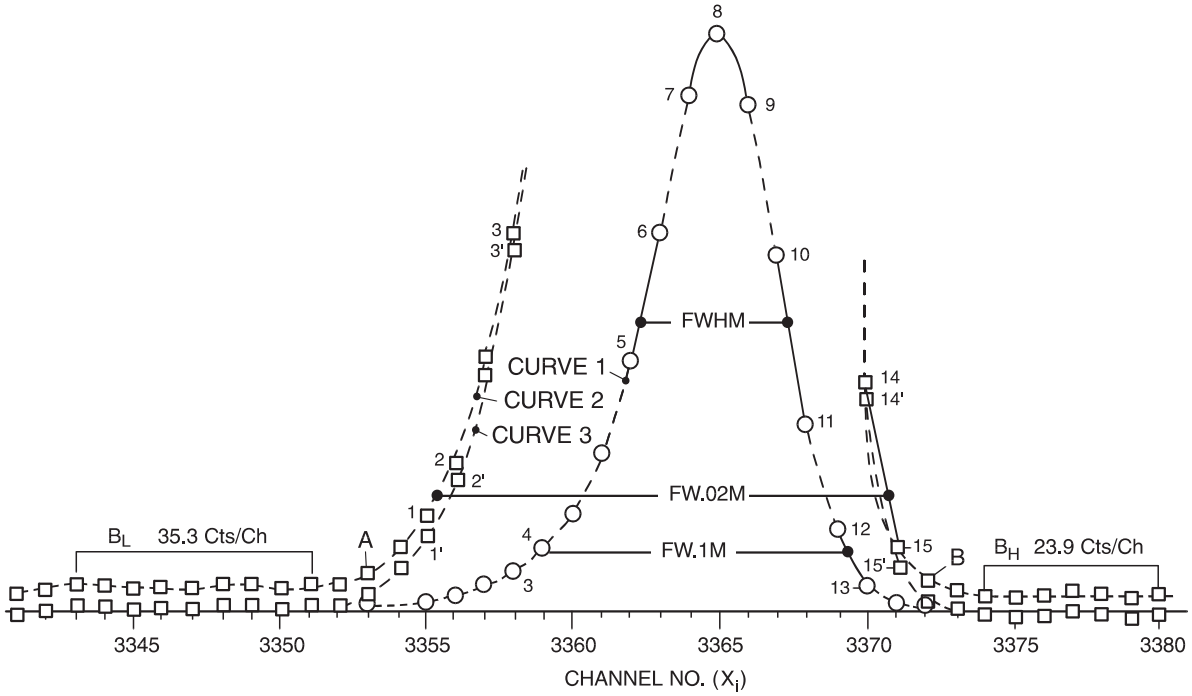

NOTE—The axes are linear. Note that the dot numbers are also the subscripts of the X and NX coordinates (channel number and counts, respectively).

Figure 7-1—1332.5 keV ^{60}Co spectral peak

[16]The spectrum was obtained with a HPGe coaxial detector having nonuniform charge collection. The evidence for nonuniformity is the skewing of the lower part of the peak towards low energies.

The photopeak (Curve 1) is approximately five channels wide across the FWHM, with the peak count in channel number 3365 of an 8192 channel ADC. A detailed description of the three curves follows:

a) *Curve 1:* The circles represent the dots seen on an MCA display, with the center channel containing 10 000 counts.
b) *Curve 2:* The vertical scale of Curve 1 was magnified 10 times to show the details at the FW.02 level. The dots in that region are represented by squares. The background counts not hidden by the peak are to the left of A (channel number 3353) and to the right of B (channel number 3372).
c) *Curve 3:* Like Curve 2, but with the background subtracted (see 7.4.1).
d) The numbered dots immediately above and below the ends of the FWHM, FW.1M, and FW.02M lines correspond to the subscripts in the N_X coordinates. These coordinates (channel numbers) and their counts, with and without background correction, appear in Table 7-2.
e) The solid line connecting dots 7–9 is a quadratic fit; the solid lines connecting dot pairs 1–2 (and 1 ft–2 ft) 3–4, 5–6, 10–11, 12–13, and 14–15 (and 14 ft–15 ft) are chords (linear fits).
f) FWHM and FW.1M are shown by the horizontal lines that terminate on the appropriate chords of Curve 1.
g) The vertical position of the FW.02M line is at 200 counts on the magnified scale (1/50th of the height of the peak channel). It can be seen that the FW.02M for Curve 2 is greater than for Curve 3, which is to be expected because Curve 2 has not been corrected for background (the lower value of FW.02M—measured at Curve 3—is the correct one).

For the calibration of the energy axis and computation of the electronic noise resolution, additional similar spectra shall be obtained for the 1173.2 keV photopeak and pulse-generator peak.

Table 7-1—Channel counts vs. channel number

Channel number	Counts	Channel number	Counts	Channel number	Counts
3343	38	3356	253	3369	1314
3344	33	3357	440	3370	393
3345	33	3358	655	3371	105
3346	34	3359	1079	3372	45
3347	38	3360	1650	3373	32
3348	42	3361	2723	3374	21
3349	44	3362	4364	3375	23
3350	36	3363	6569	3376	29
3351	44	3364	8910	3377	31
3352	42	3365	10 000	3378	28
3353	63	3366	8748	3379	20
3354	107	3367	6177	3380	27
3355	162	3368	3281	—	—

7.3 Noise resolution near 1.2 MeV

After the energy-axis and peak-resolution data have been recorded, an electronic-noise spectrum shall be obtained as follows:

a) A pulse generator shall be connected to the test-input terminal of the preamplifier (usually available at the front panel of the main amplifier), and the generator shall be adjusted so that its peak falls between the two photopeaks. Because pile-up is not a problem when using a constant-frequency

pulse generator, a counting rate ≥5000 c/s may be used. (The radioactive source may be removed if it produces a background count under the generator peak.)

b) At energies above 1 MeV, the generator peak will be so narrow that correction for the channel-width effect is mandatory (see 7.4.4).

c) If the peak positions are shifted for other measurements and a noise correction is made with the FWHM expressed in *channels*, the noise calibration shall be repeated. If the noise correction is made in *units of energy*, there is no need to repeat the calibration unless the amplifier gain is changed by more than a factor of two (see the next subclause).

7.3.1 Noise resolution near 120 keV

If the energy resolution is measured with a ^{57}Co source, a noise test can also be made with the pulser peak placed between the two lines at 122.1 and 136.5 keV. At this energy, the amplifier gain setting must be higher than for ^{60}Co, giving more channels across the peak and greater accuracy in the determination of the pulser FWHM. However, the noise computed in units of energy is likely to differ between the two measurements because the amplifier noise is, to some degree, affected by its gain.

Detector resolution corrections for electronic noise shall be based on measurements made at the same amplifier gain setting for the test source and the pulse generator.

7.4 Computations

The formulas used for computing the photopeak parameters are covered in the immediately following subclauses.

Peak positions and resolutions are computed first in units of ADC channels, then converted to electronvolts or kiloelectronvolts by multiplying by electronvolts per channel or kiloelectronvolts per channel, respectively.

7.4.1 Background correction for a continuum

The procedure described in 7.1.1 for subtracting the background can be used for a continuum as well as for an interfering peak, avoiding the need to make computations. This procedure requires two MCA runs: one with source plus background (leading to the spectrum illustrated by Figure 7-1), the other with background alone. However, the second run of the preceding case can be avoided if the first one includes at least 10 channels of background on each side of the peak, as shown by Curve 2 of Figure 7-1. In this case, the following step-by-step procedure shall be used:

a) Define
B_H as the background counts per channel (cts/ch) on the high-energy side of the peak (beyond dot B, Figure 7-1)
B_L as the background cts/ch on the low side (below dot A)
B_Δ as the difference

b) From the channel counts corresponding to the dots listed in column 3 of Table 7-2, subtract the background counts listed in column 4.

NOTE—The correction formulas shown in column 4 were derived with the assumption that the change in background from B_H to B_L under the peak is proportional to its area measured from dot B downwards to dot A (Figure 7-1). Thus, the area between dot B and the right-hand end of the FWHM line is approximately 24% of the total peak area, making the background at X_{10} and X_{11} equal to the value shown in column 4 of Table 7-2 (i.e., $B_H + 0.24B_\Delta$).

Table 7-2—Counts vs. channel number

Designated channel addresses[a]	Actual channel numbers	Channel counts (including background)	Background correction formula (subtract from column 3)[b]	Column 3 corrected for background (column 3 – column 4)
X_1	3355	162	$B_L = 35.3$	127
X_2	3356	253	$B_L = 35.3$	218
X_3	3358	655	$B_L - 0.02B_\Delta$	620
X_4	3359	1079	$B_L - 0.02B_\Delta$	1044
X_5	3362	4364	$B_L - 0.24B_\Delta$	4331
X_6	3363	6569	$B_L - 0.24B_\Delta$	6536
X_7	3364	8910	$B_H + 0.5B_\Delta$	8880
X_8	3365	10 000	$B_H + 0.5B_\Delta$	9970
X_9	3366	8748	$B_H + 0.5B_\Delta$	8718
X_{10}	3367	6177	$B_H + 0.24B_\Delta$	6150
X_{11}	3368	3281	$B_H + 0.24B_\Delta$	3254
X_{12}	3369	1314	$B_H + 0.02B_\Delta$	1290
X_{13}	3370	393	$B_H + 0.02B_\Delta$	369
X_{14}	3370	393	$B_H = 23.9$	369
X_{15}	3371	105	$B_H = 23.9$	81

[a] See Figure 7-1.
[b] B_L: Average background, low side (35.3 cts/ch)
B_H: Average background, high side (23.9 cts/ch)
B_Δ: $B_L - B_H$ (11.2 cts/ch)

Example (Refer to Figure 7-1 and Table 7-2):

B_L = 35.3 counts per channel (cts/ch), averaged over channel numbers 3342 to 3351
B_H = 23.9 cts/ch, averaged over channel numbers 3374 to 3380
$B_\Delta = (35.3 - 23.9)/2 = 11.2$ cts/ch

Table 7-2, third and fourth lines:

Dot 3 (column 1) represents 655 counts (column 3)
Dot 4 represents 1079 counts
$655 - (B_L - 0.02B_\Delta) = 619.9$ counts
$1079 - (B_L - 0.02B_\Delta) = 1043.9$ counts

Note that in Figure 7-1, only the FW.02M is significantly affected by the background.

7.4.2 Peak amplitude and peak center

The coordinates of the three dots that comprise the top of the photopeak define a quadratic equation of the following form:

$$N_X = AX^2 + BX + C \tag{7-1}$$

where

X is the channel number
N_X is the counts in the channel

By solving for *dy/dx* = 0 in Equation 7-1, Equations 7-2 and 7-3 are obtained that give the exact height $\hat{N}$ and channel number $\hat{X}$ of the peak:

$$\hat{N} = \frac{(N_7 - N_9)^2}{8(N_7 + N_9 - 2N_8)} \tag{7-2}$$

$$\hat{X} = X_7 + 1 + \frac{N_7 - N_9}{2(N_7 + N_9 - 2N_8)} \tag{7-3}$$

where

X_7, N_7, N_8, and N_9 are the coordinates of the points 7, 8, and 9 shown in Figure 7-1.

When those coordinates are entered into Equations 7-2 and 7-3, it is found that the peak channel is located at $\hat{X}$ = 3364.97 channels and the peak count is $\hat{N}$ = 9996. When corrected for channel width by Equation 7-7, $\hat{N}$ becomes 10 080 counts (see 7.4.4). The peak channel location is unaffected by the correction. *To obtain the energy of the peak, its address in channels must be multiplied by the kiloelectronvolts per channel.* The location of the peak channel is not the centroid, but when the peak is skewed towards the low-energy side (as it is in this example), the location of the peak channel is a more realistic indication of energy than the centroid.

The peak location $\hat{X}$ can fall exactly on one of the three dots or it can fall between two of them. With only five channels across the FWHM, the pattern of the dots relative to the center channel affects the resolution number by no more than 0.3%. The maximum error occurs when the peak channel is one-third of the way between two of the dots. The affect is inversely proportional to the square of the number of channels across the FWHM.

7.4.3 Resolution

With linear interpolation, dots just above and below the resolution lines in Figure 7-1 are joined by chords. FWHM, FW.1M, and FW.02M are the lengths of the respective resolution lines where they intersect those chords. Each chord can be expressed as a linear equation of the form $X_i = AN + B$, where $N = 0.5\hat{N}$, $0.1\hat{N}$, or $0.02\hat{N}$, from which the desired values of X_i can be obtained, but a preferred method is to find the X_i's by proportions as shown by Equations 7-4 through 7-6.

$$\Delta_{0.5} = (X_{10} - X_5) + \frac{N_{10} - 0.5\hat{N}}{N_{10} - N_{11}} - \frac{0.5\hat{N} - N_5}{N_6 - N_5} \tag{7-4}$$

$$\Delta_{0.1} = (X_{12} - X_3) + \frac{N_{12} - 0.1\hat{N}}{N_{12} - N_{13}} - \frac{0.1\hat{N} - N_3}{N_4 - N_3} \tag{7-5}$$

$$\Delta_{0.02} = (X_{14} - X_1) + \frac{N_{14} - 0.02\hat{N}}{N_{14} - N_{15}} - \frac{0.02\hat{N} - N_1}{N_2 - N_1} \tag{7-6}$$

In each of the equations, the first group in parentheses is the "coarse" address of the channels containing the ends of the resolution lines. The "refined" addresses are furnished by the next two fractions, which are the fractions of the channels by which the ends of the lines exceed their low-energy edges. (The subscripts refer to the dot numbers in Figure 7-1.)

7.4.4 Channel-Width correction

Corrections for finite channel width shall be made if seven or fewer channels appear across the FWHM:

a) Correct each of the channel counts for background (see 7.4.1).
b) Determine the FWHM using Equation 7-4.
c) Apply Equation 7-7 to each of the channel counts in the photopeak.
d) Using the corrected channel counts, recompute the FWHM using Equation 7-4, and compute FW.1M and FW.02M using Equations 7-5 and 7-6.

$$N_X \; N'_X \left[1 + \frac{5}{(\Delta_{0.5})^2}(0.1551 + 0.0178 \; \ln \; N'_X) \right] \tag{7-7}$$

where

N_X is the corrected count in Channel X

N'_X is the recorded count in Channel X

$\Delta_{0.5}$ is the number of channels across the FWHM

7.4.5 Energy-Axis calibration

The energy-axis calibration shall be performed as follows:

a) The addresses of the peak centers of the two calibrating peaks shall be computed using Equation 7-3. It is unnecessary to apply channel-width corrections because they do not affect the location of the peak centers.
b) The energy difference between the peaks of the test source shall be divided by the difference in channel numbers between the peak centers. The resulting number is the energy per channel.

7.4.6 Resolution with and without corrections

The results of applying the methods given in the preceding subsections to the photopeak shown in Figure 7-1 are shown in Table 7-3.

Table 7-3—Resolution with and without corrections for background and channel width

Corrections	None		Background only		Background + channel width	
Parameter	Channel	S_R[a]	Channel	S_R[a]	Channel	S_R[a]
$\hat{X}$	3364.97	—	3364.97	—	3364.97	—
FWHM	5.12	—	5.09	—	5.05	—
FW.1M	10.53	1.13	10.42	1.12	10.28	1.12
FW.02M	15.25	1.25	14.78	1.22	14.58	1.22

[a] S_R is the skewing factor FW.1M/(1.82 FWHM) or FW.02M/(2.38 FWHM). For an ideal detector, the ratio is 1.000. The amount by which the ratio is greater than 1.000 is a measure of peak spreading at 0.1 maximum or 0.02 maximum (see 6.2.2).

In Table 7-3 the uncorrected FWHM of 5.12 channels becomes 5.05 channels after applying the channel-width correction formula (change of 1.3%), the FW.1M of 10.53 channels becomes 10.28 (change of 2.4%), and the FW.02M of 15.25 channels becomes 14.58 (change of 4.6%).

The corrections exceed the target 1.2% limit-of-error stated in Clause 5.

7.4.7 Correction for electronic noise

The FWHM of the detector, corrected for internal electronic noise of the detector-amplifier system, shall be established by quadratically subtracting the FWHM of the generator peak from the measured FWHM of the detector according to

$$\Delta N_O = \sqrt{(\Delta N_S)^2 - (\Delta N_T)^2} \tag{7-8}$$

where

ΔN_O is the FWHM due to all factors other than electronic noise (channels)
ΔN_S is the FWHM of the measured γ-ray peak (channels)
ΔN_T is the FWHM of the pulser peak (channels)

In a measurement of noise in the detector that yielded the data shown in Figure 7-1, a pulser peak in channel number 7000 gave a FWHM of 3.376 channels (corrected for channel width using Equation 7-7). The photopeak gave a FWHM of 10.52 channels. Corrected for the electronic noise by using Equation 7-8, the resolution becomes 9.96 channels FWHM (change of 5.3%). When the Figures are multiplied by 0.190 keV per channel for this measurement, the noise becomes 0.65 keV FWHM, the uncorrected detector resolution becomes 2.00 keV FWHM, and the corrected resolution becomes 1.89 keV FWHM.

8. Energy rate limit

With a resistor-feedback preamplifier that is dc-coupled to a detector, the ionization current from the crystal flows through the feedback resistor, causing the dc level at the output to change. Superimposed on that change is a random fluctuation of voltage having an rms value proportional to $n^{1/2}$ where n is the counting rate (c/s). With a sufficiently high counting rate, the peaks of the output pulses riding on the dc level will saturate the preamplifier (IEEE Std 301-1988). The limiting energy times the count-rate is known as the ERL.[17]

With an ac-coupled preamplifier, the dc component is missing, but the statistical fluctuations remain. For slow changes in counting rate, saturation does not occur until the rate is much greater than for the dc-coupled case. The limiting situation is known as the E^2RL. For rapid changes in rate (as may occur in particle accelerator measurements) the dc condition applies.

Preamplifiers that are ac-coupled are no longer supplied by manufacturers of germanium detectors; the E^2RL will not be further addressed in this standard.

For preamplifiers dc-coupled to the detector (and for ac-coupled preamplifiers subjected to bursts of counting rate) the ERL is given by

$$\mathrm{ERL} = (6.25\ \varepsilon\ V_{\mathrm{m}} \cdot 10^{12})/R_{\mathrm{f}} \qquad (8\text{-}1)$$

where

ERL is the energy × counting rate (MeV · c/s)
ε is the electronvolt per hole-electron pair (ε = 3.0 for Ge)
V_{m} is the linear maximum output of the preamplifier (in volts)
R_{f} is the feedback resistor (in ohms)

See IEEE Std 301-1988 for the method of determining the size of a feedback resistor when the resistor is sealed in a cryostat.

9. Peak-to-Compton ratio

The importance of having a high P/C is given in 4.1.2.

For a given geometry, the P/C is inversely proportional to resolution and generally increases with increasing efficiency, approximately as the 0.3 power. The P/C is reduced by Compton scattering in material near the detector or source, including material in the detector-element mounting assembly.

The P/C shall be measured for the 1.332.5 MeV peak of the ^{60}Co spectrum. The procedure given in Clause 7 shall be used for recording the spectrum, which shall extend downwards to below 1 MeV (see Figure 9-1). Then,

a) The number of counts $\hat{N}$ in the peak channel shall be determined at channel number $\hat{X}$.
b) The average number of counts per channel N_{c} between 1040 keV and 1096 keV of the Compton spectrum shall be determined (see Figure 9-1). Note that this region avoids the Compton edge that occurs at

[17]Reset-type preamplifiers, in principle, cannot be saturated because they reset when the dc output level exceeds a predetermined level. This allows the counting rate to be much higher for a reset-type unit than for a resistor-feedback type. However, if linear shaping networks are used in the main amplifier, pulse pile-up will eventually degrade the energy resolution to an unacceptable degree. The concept of ERL described in this standard does not apply to reset-type preamplifiers.

$$E_C = \frac{2E^2}{2E + 511} \tag{9-1}$$

where E is the energy of the peak in kiloelectronvolts.

c) A correction shall be made to N_c and $\hat{N}$ for the natural background counts, but not for the background caused by scattering of photopeak counts. The natural background is determined from the counts obtained with the source removed.

The P/C is defined as the ratio of the counts obtained in step a) to those in step b).

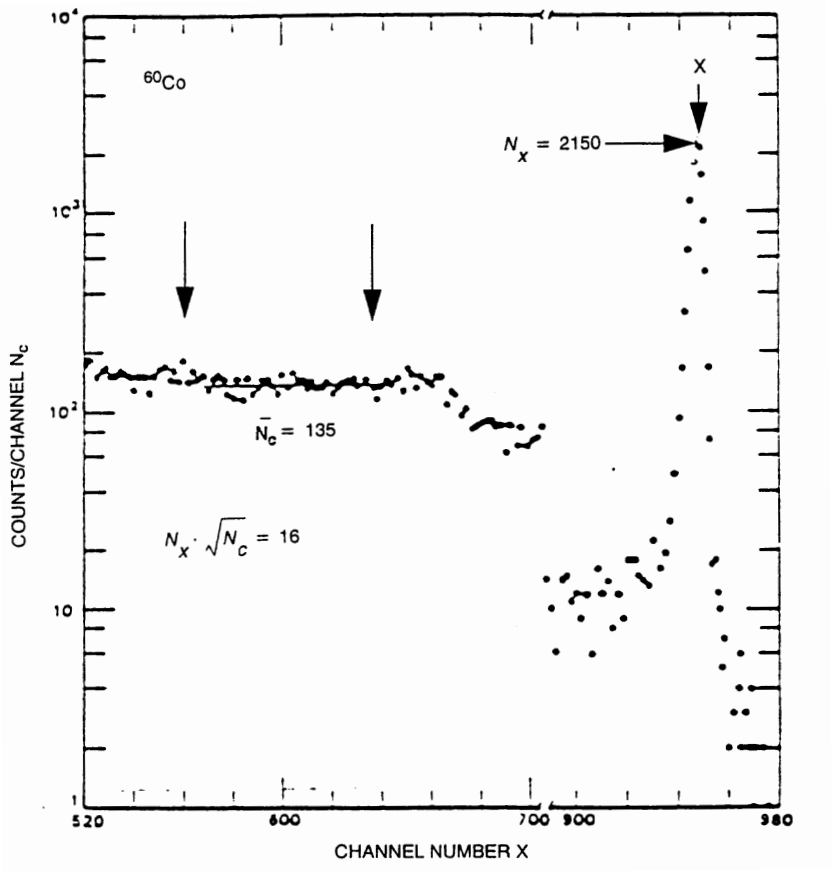

Figure 9-1—^{60}Co gamma-ray spectrum showing determination of peak-to-Compton ratio

10. Counting efficiency

The gamma-ray counting efficiency for a full-energy peak or an escape peak depends upon the active volume of the detector, its shape, source-detector geometry, and the interactions with the material in the immediate vicinity of the detector, including the crystal mount and the cryostat parts. The efficiency is defined for the complete detector assembly.

Several detector efficiency specifications are widely recognized:

a) Absolute efficiency of a planar or coaxial detector, point source 25.0 cm from the center of the front of the detector endcap (see 6.2.6 and 6.2.7)
b) Efficiency of a coaxial detector relative to that of a 76 mm × 76 mm (3 in × 3 in) NaI(Tl) detector, point source 25.0 cm from the center of the front of the detector endcap (see 6.2.6 and 6.2.7)
c) Absolute efficiency when using a reentrant (Marinelli) beaker, standard source placed over the detector endcap (see 10.6)
d) Absolute efficiency of a well-type detector, point source on the axis of symmetry 1.0 cm from the bottom of the well (see 10.4)

The above-specified geometries provide a basis for testing, comparing, and selecting detectors for most applications. In practice, other geometries such as a bottle placed on the endcap or a mini-Marinelli beaker (diameter greater than the length) may be used. For any efficiency quoted as a specification, the type of efficiency measurement shall be clearly stated.

Methods of testing are given in the following subclauses.

10.1 Absolute counting efficiency for a full-energy peak

With the setup shown in Figure 5-1, obtain a spectrum using a calibrated ^{60}Co source (see Clause 7). The source-to-cryostat endcap distance measured from the center of the source to the center of the front of the endcap shall be 25.0 cm. The absolute peak counting efficiency is

$$\eta_a = 100 \cdot [A / N_s] \quad (10\text{-}1)$$

where

η_a is the absolute counting efficiency (%)
A is the counts in the full-energy peak, less background (see the next subclause)
N_s is the total number of 1.332.5 keV photons emitted by the source during the live counting time

Instead of depending on the live-time clock in the MCA, the counting time may be determined from the area of a pulser peak located ≈5% above the ^{60}Co line if the pulse rate is known.

For applications in which a source will be placed close to the endcap, an additional absolute efficiency measurement simulating that condition may be useful.

10.2 Background correction

In making a correction for the background, the required steps are as follows:

a) To establish a region of interest (ROI) that defines the boundaries of a peak
b) To determine the total counts (peak plus background) within the ROI
c) To determine the background counts within the ROI

d) To subtract the background from the total to establish the net counts in the peak

There are MCAs with built-in routines for doing the preceding; the purpose of 10.2.1–10.2.2 is to furnish the information in the absence of such a routine, and to check the routine if it exists in the MCA.

10.2.1 Background correction, procedure 1

Use the method in 7.1.1.

This method shall be used if there is a background peak that overlaps the test-source peak; the method is optional if the background contains no such peak.

If the method of 7.1.1 is used, the edges of the ROI may extend several channels beyond the ends of the peak without causing an error (because the extra channels will not contribute counts).

With the background subtracted as described above, the counts in the peak shall be determined by summing the counts in all of the channels within the ROI.

10.2.2 Background correction, procedure 2

Use the longer of the two methods referred to in 7.4.1 (the “single-run” method). Proceed as follows:

a) From Table 7-2 and Figure 7-1, note that B_L = 35.3 cts/ch and B_H = 23.9 cts/ch.
b) Find the channel address on both sides of the peak where the channel count begins to rise above the average background level. On the low side of the peak, that address is channel number 3353 (A in Figure 7-1). On the high side, the address is channel number 3372 (B in Figure 7-1). Those channel addresses define the ROI.
c) Sum the counts within the ROI (channel numbers 3354 to 3372 in Table 7-1; 3353 is the 0th channel of the ROI); that sum is 56 980 and includes the background.
d) Compute the background counts by averaging B_L and B_H, then multiplying by the number of channels within the ROI,

$$\text{Background} = 0.5(B_L + B_H) + (X_B - X_A)$$
$$= 562 \text{ counts}$$

where X_B and X_A are the upper and lower bounds of the peak (channel numbers 3372 and 3353, respectively).
e) Subtract the background counts from the total to yield

56 980 total
562 background
50 418 net counts.

Note that if the channel boundaries of the ROI were chosen as 3355 and 3371—a change of one channel in the direction to maximize the error at each boundary—the results would be

56 876 total
474 background
50 402 net counts,

a difference of 16 counts from the preceding net—substantially less than the standard deviation of the net counts in the peak (σ = 225)—a figure that sets a limit of acceptable error.

The acceptable error in judgement in setting the boundaries of the ROI depends on the background count relative to the total count in the peak, and on the curvature of the peak boundaries at the background level.

10.3 Relative full-energy peak counting efficiency

The full-energy peak counting efficiency relative to that of a 76 × 76 mm (3 in × 3 in) NaI (Tl) scintillation crystal at a source-to-detector distance of 25.0 cm shall be determined from

$$\eta_{rel} = 100 \cdot [A / A_{NaI}] \quad (10\text{-}2)$$

where

η_{rel} is the relative efficiency (%)

A is the counts in the full-energy peak, less background

A_{NaI} is $1.2 \cdot 10^{-3} N_s$ for the 1332.5 keV gamma-ray emitted from ^{60}Co at a source-to-endcap distance of 25.0 cm

10.4 Well-Type coaxial detector efficiency

A well-type coaxial detector has a reentrant cavity in the endcap that extends into a central hole in the detector element. The hole may be a blind hole (see Figure 4-3) or a through hole. A source placed in the well is nearly surrounded by active germanium, maximizing the absolute counting efficiency, particularly with blind-hole geometry. Placing the source inside the well also results in the summing of coincident gamma rays to a much greater degree than sources located outside.

10.5 Summing of coincident gamma rays

If the source contains pairs of coincident gamma rays, a significant sum peak appears in the spectrum, with each count in the sum peak representing the simultaneous full-energy detection of both gamma rays. Also present will be a continuum below the sum peak, with each count in the continuum produced by a Compton event from one of the pair and a full-energy event from the other.

It is very important to include in the calculations of efficiency the counts falling into the energy region above the primary peaks, because to ignore them is to cause the computed efficiency to become progressively deficient as the real efficiency increases. The way to deal with this situation is too complex to be treated in this standard; the reader is referred to [B3].

10.6 Detector gamma-ray efficiency with a Marinelli reentrant beaker

Because of the need in many studies to measure the activity of a large-volume, low-activity sample [B11] in liquid form, it is desirable to enhance the detection efficiency by surrounding the detector element with the sample, rather than by just placing it on top. This is accomplished with a Marinelli (reentrant) beaker.[18]

The placement over a detector endcap is shown in Figure 10-1(A).

[18] Maximum efficiencies occur for the Model 450 and Model 1000 beakers when the height of the liquid above the reentrant plane of the beaker approximately equals *W*. (In Figure 10-1B, that liquid surface is at $H_2 + t_3 + W$.) When filled to nominal capacity, the beaker designs reflect this condition.

Two beaker geometries are designated as standard: Model 450 and Model 1000, in accordance with Figure 10-1B); the dimensions are given in Table 10-1. The nominal capacities are 450 mL and 100 mL, respectively, though, when full, they can hold about 640 and 1570 mL, respectively. Many other beaker geometries are available (see Annex A), the choice of which to use depends on the size of the sample and the need to place it as close to the detector element as feasible, thereby maximizing the counting efficiency.

The spectrometer shall be set up and calibrated as specified in Clause 7. The source shall contain a prominent peak not in coincidence with any other. Coincidence or Compton suppression modes shall not be used.

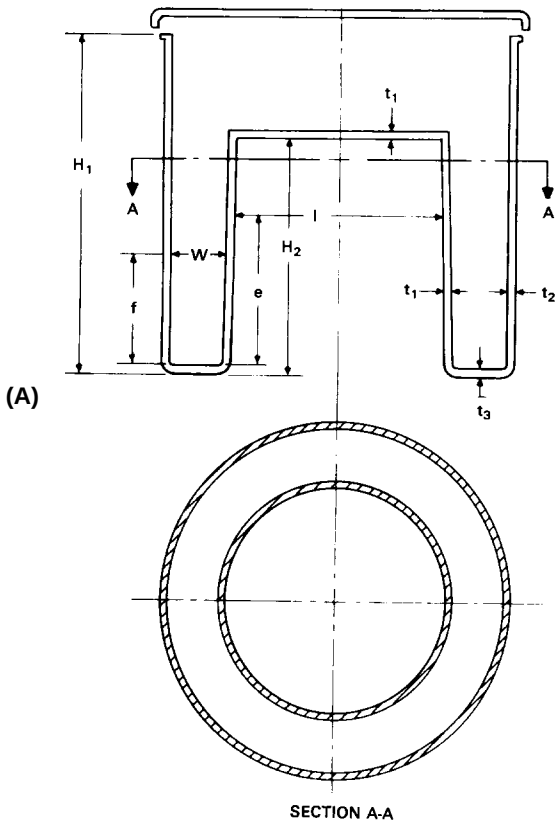

MODEL 450		
	mm	in
H_1	104.1 ± 1.3	4.10 ± 0.05
H_2	68.33 ± 0.15	2.690 ± 0.006
l	[77.40 − 0.008e] ± 0.10 AVERAGE ± 0.25 MAXIMUM	[3.048 − 0.008e] ± 0.004 AVERAGE ± 0.010 MAXIMUM
W	[14.83 + 0.008f] ± 0.10 AVERAGE ± 0.25 MAXIMUM	[0.584 + 0.008f] ± 0.004 AVERAGE ± 0.010 MAXIMUM
t_1	1.90 ± 0.1	0.075 ± 0.004
t_2	2.00 ± 0.25	0.079 ± 0.010
t_3	3.60 ± 0.15	0.142 ± 0.006

MODEL 1000		
	mm	in
H_1	150.0 ± 1.3	5.91 ± 0.05
H_2	100.00 ± 0.15	3.937 ± 0.006
l	[120.00 − 0.008e] ± 0.1 AVERAGE ± 0.25 MAXIMUM	[4.724 − 0.008e] ± 0.004 AVERAGE ± 0.010 MAXIMUM

ALL OTHER DIMENSIONS SAME AS FOR MODEL 450.

MATERIAL: PLASTIC OF DENSITY 1.1 ± 0.1.

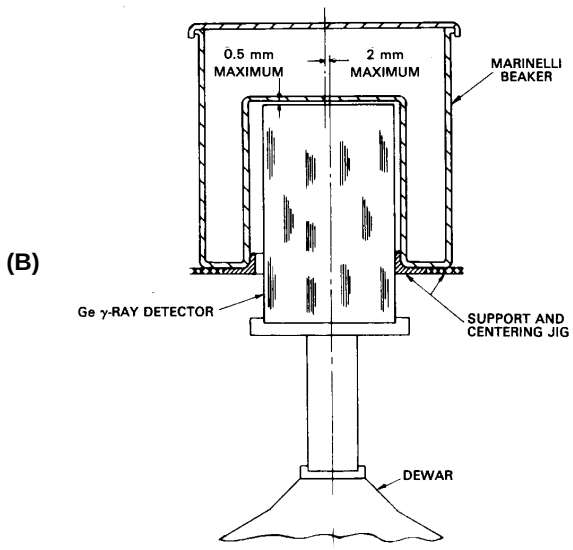

Figure 10-1—Marinelli beaker with germanium detector

**Table 10-1—Standard Marinelli (reentrant) beakers
Models 450 and 1000 (Dimensions refer to Figure 10-1)**

Model 450		
Parameter	**Size (mm)**	**Size (in)**
H_1	104.1 ±1.3	4.10 ± 0.05
H_2	68.33 ± 0.15	2.690 ± 0.006
D_1	76.85 ±0.10 average ±0.25 maximum	3.026 ±0.004 average ±0.01 maximum
D_2	77.40 ±0.10 average ±0.25 maximum	3.048 ±0.004 average ±0.01 maximum
t_1	1.90 ± 0.10	0.075 ± 0.004
t_2	2.00 ± 0.25	0.079 ± 0.010
t_3	3.60 ± 0.15	0.142 ± 0.006

Model 1000		
Parameter	**Size (mm)**	**Size (in)**
H_1	150.1 ±1.3	5.91 ± 0.05
H_2	100.00 ± 0.15	3.937 ± 0.006
D_1	119.20 ±0.10 average ±0.25 maximum	4.693 ±0.004 average ±0.01 maximum
D_2	120.00 ±0.10 average ±0.25 maximum	4.724 ±0.004 average ±0.01 maximum
t_1	1.90 ± 0.10	0.075 ± 0.004
t_2	2.00 ± 0.25	0.079 ± 0.010
t_3	3.60 ± 0.15	0.142 ± 0.006

Material: Plastic of density 1.1 ± 0.1

10.7 Marinelli beaker standard source (MBSS)

A Marinelli beaker standard source (MBSS) consists of a Standard Marinelli Beaker (see 10.6) containing a carrier with radioactive material (see 10.7.6). Four categories are recognized: a certified MBSS, a calibrated MBSS, a certified-solution MBSS, and a calibrated-solution MBSS.

The calibration uncertainty of the photon emission rate[19] for the filled beaker shall be less than 3% unless otherwise stated.

10.7.1 Certified MBSS

A certified MBSS is an one that has been calibrated for photon emission rate[20] at specified energies by a laboratory recognized as a country's national standardizing laboratory for radioactivity measurements[21] and has been so certified by the calibrating laboratory.

10.7.2 Calibrated MBSS

A calibrated MBSS is one that has been calibrated by comparing its photon emission rate to that of a certified MBSS.

10.7.3 Certified-Solution MBSS

A certified-solution MBSS is a standard beaker conforming to 10.6 that contains a certified solution (see 10.7.5) as its radioactive filling material (see 10.7.6).

[19]The photon emission rate used in this standard is the number of photons per second resulting from the decay of radionuclides in the source and is thus higher than the detected rate at the surface.

[20]International Commission on Radiation Units and Measurements, Certification of Standardized Radioactive Sources, ICRU Report no. 12, Sept. 15, 1968.

[21]For the U.S., the National Institute of Standards and Technology is the certifying laboratory.

10.7.4 Calibrated-Solution MBSS

A calibrated-solution MBSS is a standard beaker conforming to 10.6 that contains as its radioactive filling material (see 10.7.6) a solution that has been calibrated by comparing its photon emission rate at specified energies to that of a certified solution (see 10.7.5).

10.7.5 Certified solution

A certified solution is a radioactive material in liquid form (see 10.7.6) that has been calibrated and certified by a laboratory recognized as a country's national standards laboratory for radioactivity measurements.

10.7.6 Radioactive filling material

The beaker used for calibration of detectors with diameters of 76.5 mm or less shall correspond to the first one listed in Table 10-2, filled with 450 mL ± 2 mL of a solid or liquid carrier containing uniformly dispersed radioactive material. For detector diameters larger than 76.5 mL, the standard beaker shall correspond to the second one in Table 10-2 and shall be filled with 1000 mL ± 2 mL.

The solid carrier is preferred for general use because it is in the form of a safe, chemically inert sealed source.

Representative radionuclides for use in MBSSs are listed in Table 10-2. The carrier shall have an effective atomic number Z of 4.0 ± 0.7 and a mean specific gravity of (1.15 ± 0.02) g cm^{-3} for solid carriers, or (1.06 ± 0.01) g cm^{-3} for liquid carriers. The density of the carrier shall be stated (see 10.9) so that attenuation corrections may be made. The source activity shall be low enough to be within the count-rate capability of the detector system (see 6.2.10).

Table 10-2—Representative radionuclides for MBSS [B24]

Parent radionuclide	Energy (keV)	Half-Life	Typical MBSS initial emission rate (ys^{-1})
^{109}Cd	88.0	463.3 days	2000
^{57}Co	122.1	272.1 days	250
^{139}Ce	165.9	137.7 days	200
^{203}Hg	279.2	46.62 days	600
^{113}Sn	391.7	115.1 days	1000
^{137}Cs	661.7	30.16 years	500
^{88}Y	898.0	106.6 days	3500
^{60}Co	1173.2	5.271 years	1500
^{60}Co	1332.5	5.271 years	1500
^{88}Y	1836.0	106.6 days	4000

10.8 Measurement, absolute efficiency, full-energy peak

The absolute efficiency of the full-energy peak of a detector assembly shall be determined with the MBSS placed over the endcap as in Figure 10-1, counted for a live time count interval *t*. The efficiency η_a is defined as

$$\eta_a = 100 \cdot [A / N_s] \quad (10\text{-}3)$$

where

η_a is the absolute efficiency, full-energy peak (%)

A is the number of events from the MBSS registered as counts in the full-energy peak at energy E during the live-time count interval t

N_s is the number of gamma rays of energy E originating in the MBSS during the same live time interval t

When the MBSS efficiencies are specified, the energies used for the determination shall be stated (see Tables 10-2 and 10-3). The 1332 keV gamma ray of ^{60}Co has been the most widely used for specifying efficiency and resolution at high energy. At low energy the preferred peak is the 88 keV gamma ray of ^{109}Cd. (Mixed sources are available that include the above energies plus others.) By using additional peaks a detailed calibration curve can be established for specific applications. An example showing typical results obtained with two germanium detectors having different efficiencies is compiled in Table 10-3.

Table 10-3—MBSS absolute efficiencies η_a (full-energy peak, total absorption) of two germanium detectors

Energy (keV)	η_a for Detector 1 (η_{rel} = 11.4%)[a]	η_a for Detector 2 (η_{rel} = 24.5%)[a]
88.0	0.025	0.0414
122.1	0.032	0.0484
165.9	0.0236	0.0368
279.2	0.0157	0.0260
391.7	0.0112	0.020
661.6	0.0068	0.0131
898.0	0.0050	0.0097
1173.2	0.0039	0.0077
1332.5	0.0034	0.0070
1836.0	0.0026	0.0054

Detector characteristics	Detector 1	Detector 2
Resolution at 1.33 MeV	1.88 keV	2.04
η_{rel}[a] at 1.33 MeV	11.4%	24.5%
Peak/compton at 1.33 MeV	44/1	50/1
Diameter	41.2 mm	53.5 mm
Length	47.5 mm	53.0 mm
Diffusion depth	1000 μm	1500 μm
Core diameter	5.0 mm	9.0 mm
Active volume	56.2 cm^3	103.8 cm^3
Surface area exposed to beaker	74.8 cm^2	111.6 cm^2

[a] η_{rel}: total absorption detector efficiency relative to that of a 76 × 76 mm (3× 3 in) NaI(Tl) scintillation crystal at a source to detector distance of 25 cm, where the peak area for the NAI(Tl) crystal is taken as $1.2 \cdot 10^{-3} N_s$. N_s is the total number of 1332.5 keV gamma-ray photons emitted by the source during the live counting time.

Figure 10-2 shows the variation of the absolute efficiency η_a (full-energy peak, total absorption) plotted for the two detectors of Table 10-3.

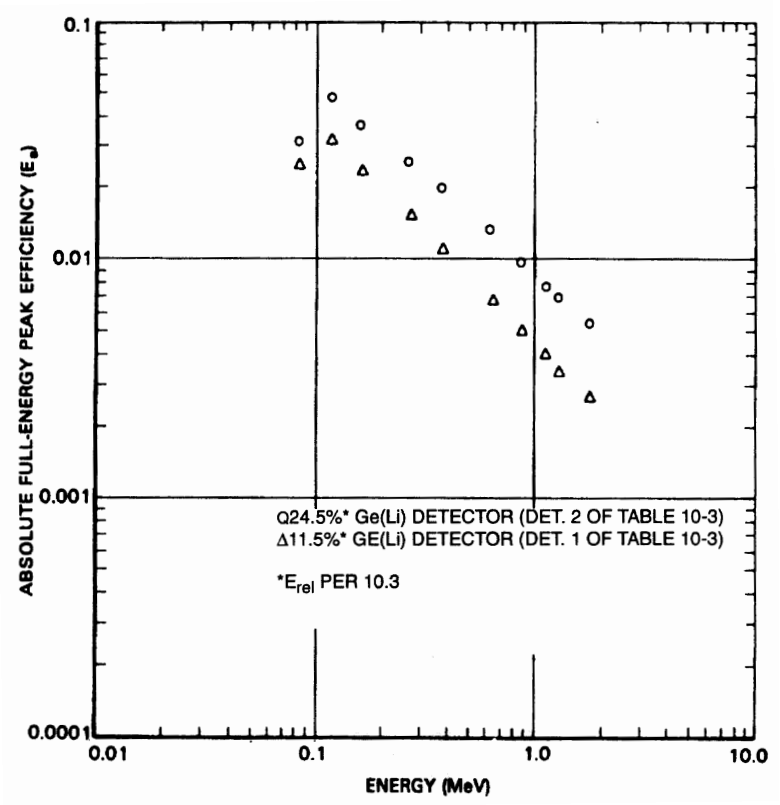

Figure 10-2—MBSS absolute efficiencies η_a (full-energy peak, total absorption) of two germanium detectors vs. energy

Figure 10-3 shows a linear plot of the MBSS spectrum (Detector 2 of Table 10-3).

Figure 10-4 shows a log plot of the MBSS spectrum (Detector 2 of Table 10-3).

Most of the peaks are clearly discernible. However, the close spacing of the ^{88}Y single escape peak at 1325 keV to the ^{60}Co peak at 1332.5 keV can cause an error. (Figure 10-5 shows an expanded portion of the spectrum around 1332 keV.) Care should be taken to avoid attributing the ^{88}Y peak to the ^{60}Co peak. Also, the ^{60}Co gamma rays at 1173.2 keV and 1332.5 keV are in prompt cascade and can sum, resulting in an error of as much as 5%. Approximate correction factors can be determined from a knowledge of the peak-to-total ratios for the secondary gamma and the gamma-gamma angular correlation. A similar situation exists for all radionuclides emitting gamma rays in prompt cascade.

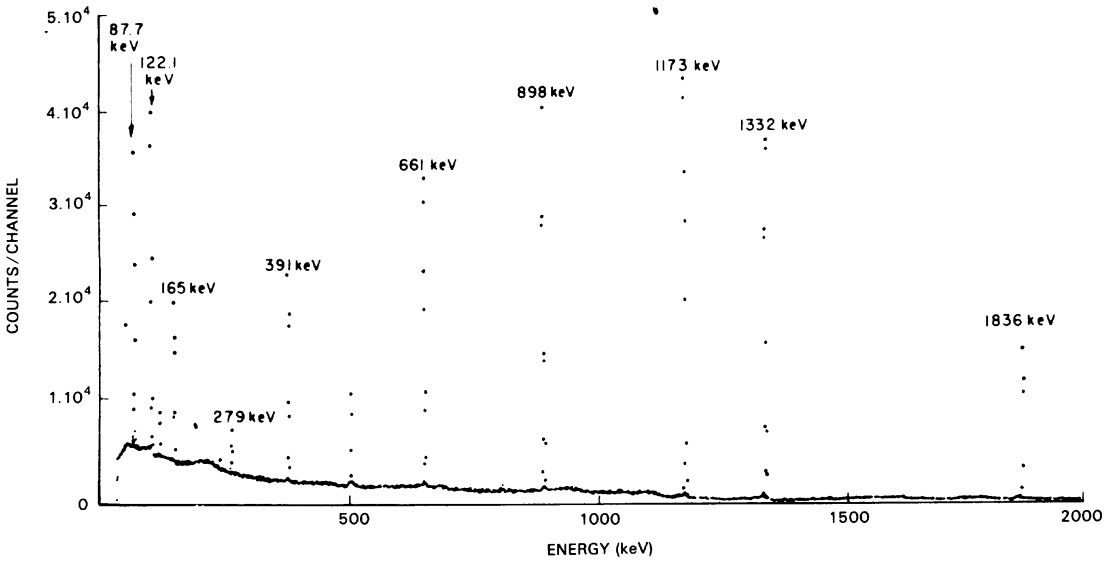

Figure 10-3—Linear plot of spectrum observed with a germanium detector using an MBSS (Detector 2 of Table 10-3)

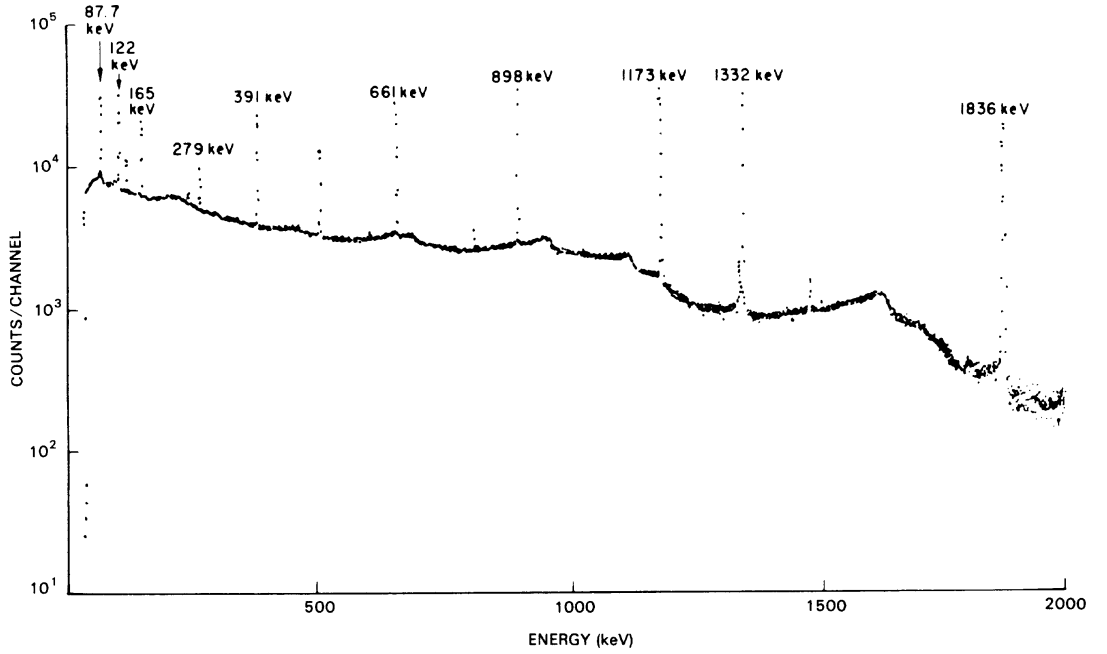

Figure 10-4—Log plot of spectrum observed with a germanium detector using an MBSS (Detector 2 of Table 10-3)

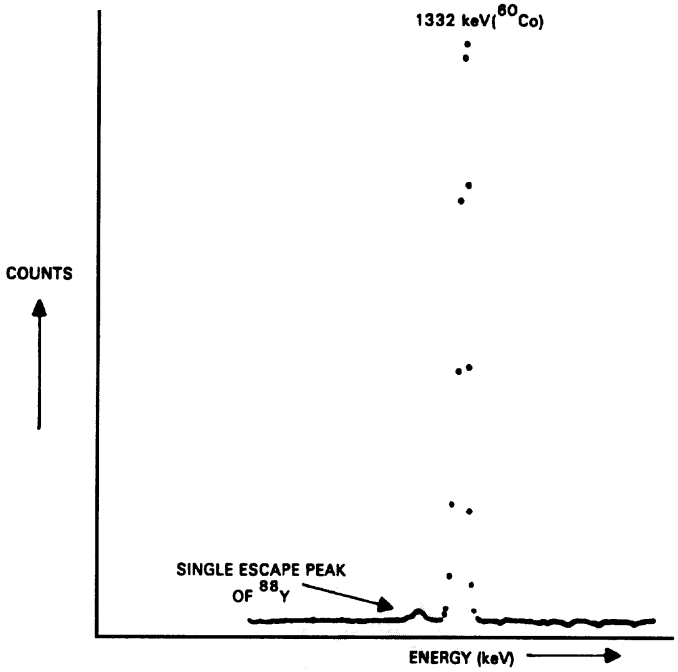

Figure 10-5—Expanded portion of Figure 10-3, 10-4 spectrum showing the 1332 keV peak of ^{60}Co and the 1325 keV single-escape peak of ^{88}Y

10.9 MBSS documentation

A certificate shall be provided with each MBSS stating whether it is a certified MBSS (see 10.7.1) or a calibrated MBSS (10.7.2). ln the case of the certified-solution MBSS (10.7.3) and the calibrated-solution MBSS (10.7.4), the certificate shall be for the solution alone. The certificate shall contain the following information:

a) Radionuclides used and calibrated together with
   1) The photon energies and radionuclide half-lives.
   2) Dates corresponding to the stated photon emission rates.
   3) Uncertainties in the stated photon emission rates; in the case of a calibrated MBSS that has been calibrated against a certified MBSS, the uncertainties for each shall be given separately; in the case of a calibrated-solution MBSS that has been calibrated against a certified-solution MBSS, the uncertainties for each shall be given separately.
   4) Density of the carrier.

b) Calibration dates: In the case of an MBSS calibrated against a certified MBSS, the dates of calibration of each shall be given; in the case of a calibrated-solution MBSS calibrated against a certified solution, the dates of calibration of each shall be given.

c) Full genealogy in the case of a calibrated MBSS or a calibrated-solution MBSS, including identification of the certified MBSS or certified solution against which it has been calibrated.

d) Calibrating laboratory or organization.

11. Window thickness index

Information on the thickness of the detector window (detector dead-layer, cryostat mount, and endcap) can be obtained by measuring and reporting a window thickness index as the ratio of peak areas. A useful radionuclide for this purpose is ^{109}Cd, which has peaks at 22 and 88 keV. For the test to be valid, self-absorption in the source and its housing must be negligible.

A window-thickness index based on X-ray fluorescence shall be used for measuring thin windows. Such an index is described in IEEE Std 759-l984. The thickness index is based on the X-ray fluorescence of a standard glass, designated SHM-47, developed by and available from the National Institute of Standards and Technology. This glass contains oxides of Si, Ba, Ca, Li, Mg, Zn, and B. When fluoresced with an ^{55}Fe source, the glass emits X-ray lines in the region from 1–5 keV. Ratios of these lines to the coherently backscattered 5.9 keV line from the source are used to define a window thickness index. Refer to IEEE Std 759-1984 for details.

12. Timing

The velocities of electrons and holes in a germanium detector are somewhat different, but both are in the vicinity of 10^7 cm/s with normal bias applied. When a hole-electron pair is generated in a detector, the hole begins travelling to the negative contact (electrode), while the electron moves in the opposite direction. When one of the charges reaches a contact, its drift through the crystal lattice is terminated, abruptly reducing the induced current and the rate-of-rise of the output signal that flowed while both charges were moving.

For a hole-electron pair generated near the center plane between two contacts 1 cm apart, the collection time is ≈50 ns. If the pair is generated near one of the contacts, the collection time increases because one of the pair must travel the full distance between contacts. The variation in collection time [B16] adversely affects the ability to establish a time marker keyed to the time-of-arrival of a gamma ray or X ray. Setting the threshold of a simple discriminator to a level just above the noise level minimizes the timing walk of the output signal (see Clause 3 for terminology), but the walk can be much reduced through the use of more sophisticated discriminator circuits. Three popular ones are the crossover-pickoff, extrapolated-zero, and the constant-fraction discriminator (CFD). The first is ruled out because it requires bipolar shaping and incurs a noise penalty, both in energy resolution and timing jitter. The second works well, but the third is most popular. In this circuit, an inverted and delayed output signal from a fast-rise preamplifier is combined with a fraction of the undelayed signal to produce a baseline crossing shortly after the initial delay. A discriminator designed to give an output signal keyed to the baseline crossing must be used with this arrangement. If the delay and the fraction are chosen correctly, timing walk less than 5 ns can be obtained with a detector of 50% relative efficiency irradiated with 511 keV gamma rays.

12.1 Setup for timing measurements

The block diagram of a system for testing the timing performance of a germanium detector [B16] is shown in Figure 12-1. The system has two paths: a start path that generates a start pulse for a time-to-amplitude converter (TAC), and a stop path in which the detector under test initiates the stop signal for the TAC. The signals for both paths are initiated by a ^{22}Na source that produces two coincident 511 keV gamma rays traveling in opposite directions (positron annihilation radiation).

The detector for the start side is a plastic scintillator coupled to a fast photomultiplier (PMT); the risetime of the combination is typically ≤5 ns. The output of the PMT passes through a CFD, a time-pickoff control, an adjustable delay box, and then to the START input of the TAC. The delay box is used to calibrate the time axis of the TAC.

The detector under test in the stop path sends its signal to a fast preamplifier, then to a fast shaping amplifier in which the differentiating time constant is made equal to the fastest risetime observed at the output of the preamplifier, then to a second CFD, and finally to the STOP input of the TAC. This CFD should be set at a signal fraction of 20%; the delay should be set at half the fastest risetime observed at the output of the preamplifier. These settings minimize walk and jitter caused by variations in detector risetime and signal amplitude.

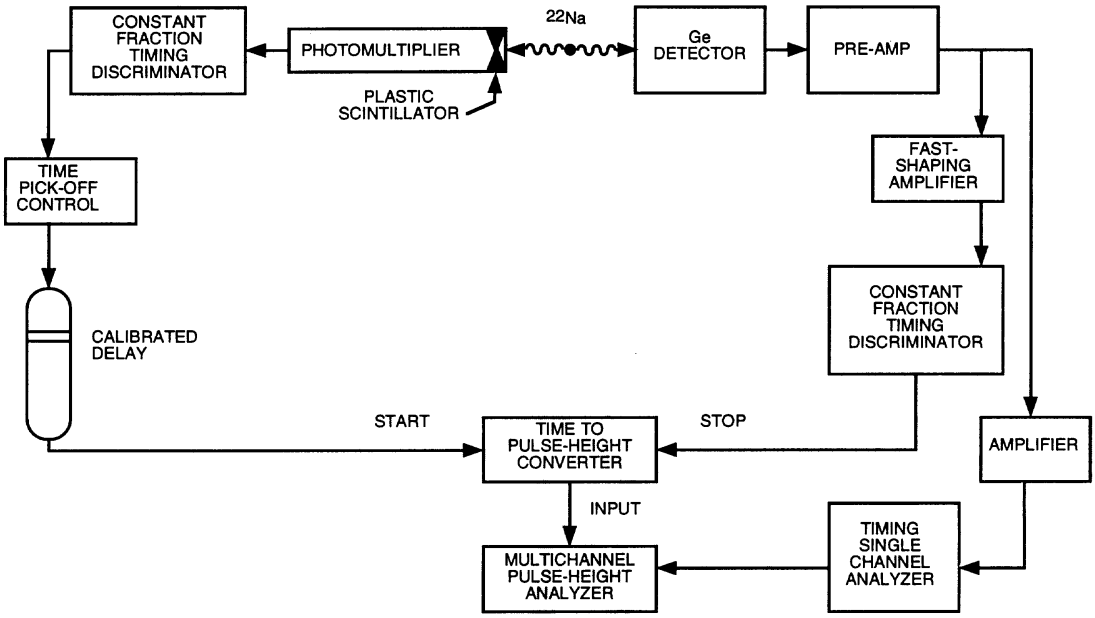

Figure 12-1—Block diagram of timing-measurment setup

A second path from the output of the preamplifier goes to an amplifier, then to a timing single-channel discriminator (TSCA), and finally to the GATE input of an MCA (its linear-signal input receives the linear output of the TAC). The TSCA acceptance window should be centered on the 511 keV gamma signal with a window width of 10%. Signals that pass through the window open the gate of the MCA, allowing it to accept signals from the TAC.

12.2 Timing measurements

Using a system like that of Figure 12-1, a gamma-ray coincidence spectrum shall be obtained as shown in Figure 12-2. The TAC sensitivity shall be adjusted to produce at least six channels between the FWHM boundaries, and the total number of counts contained within the FWHM shall be at least 4000. Fewer than 4000 counts may be accumulated if the dispersion of the FWHM is <5% with a 90% confidence level. After calibrating the time-axis with at least two known delays, the FWHM and the FW.lM shall be measured in units of nanoseconds. The following parameters shall be given with the results of the test:

a) Detector bias
b) Differentiation time of the fast shaping amplifier
c) Shaping delay time

Timing measurements are dependent on the entire electronics system and its adjustment, which is critical and difficult. It can be assumed that the measured timing characteristics represent an upper limit to those of the detector alone.

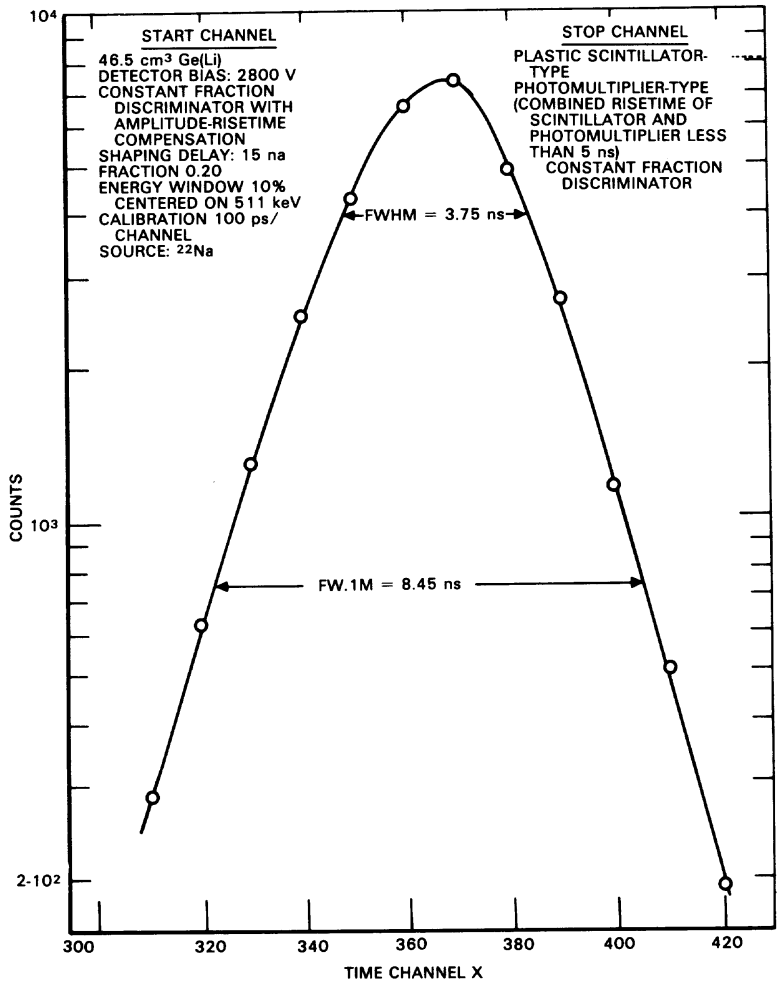

Figure 12-2—Gamma-Ray coincidence spectrum showing resolving-time dispersion of a detector

13. Temperature-Cyclable detectors

Cyclable detectors are those that can be allowed to warm up to room temperature when not in use (after reducing the bias to zero), then cooled to LN temperatures when needed for measurements. While warm, the detector remains under vacuum as an integral part of the cryostat system.

To designate a detector as cyclable, a manufacturer shall guarantee that the detector meets its performance specifications throughout the warranty period even if cycled an unlimited number of times between room temperature and the operating temperature, if done so according to the manufacturer's instructions. It shall also be guaranteed that the detector can be stored at room temperature throughout the warranty period.

14. Annealable detectors

A high-temperature bake (annealing) can restore many HPGe detectors damaged by radiation to a performance level approaching that of new ones [B2]. Neutron damage in conventional-electrode geometry coaxial detectors (p-type) can result in a greater loss of efficiency than in reverse-electrode types (n-type). Also,

because n-type detectors are less sensitive to small amounts of residual damage than p-type, they are easier to restore to their original condition. In a typical annealing cycle, the detector is baked at 100 °C to 120 °C for 24 h while the cryostat is evacuated with an extremely clean pumping system.

To designate a detector as annealable, a manufacturer shall state that in the absence of radiation damage, the detector will tolerate the annealing schedule and still meet its original warranted performance.

15. Low-Background detectors

Ambient background counts in a detection system sets the limit of sensitivity in the measurement of radioactive samples. When the sample activity approaches the level of naturally occurring radioactivity, extreme measures are necessary to reduce the background of the measuring system.

The major contributors to ambient background are cosmic rays and the radioactive contaminants present in the construction materials of the counting room, shield, and detector. The effect of the contaminants depends on their energy, abundance, and proximity to the detector. Nuclides that are part of a radioactive parent/daughter chain will not necessarily be in equilibrium—the background may change with time as equilibrium is approached. Furthermore, sampling the raw construction material for contaminants prior to processing may lead to surprises—the constituents may be affected differently by the processing, thereby altering a parent/daughter fraction.

Another item affecting the background is the sample blank: if some of the naturally occurring radiation can scatter from the blank into the detector, the background counts will increase; if the blank helps shield the detector, they will decrease.

Low-background detectors are typically constructed from selected materials having radionuclide concentrations known to be lower than those used in standard detector assemblies. The materials are sampled and assayed for contaminating radionuclides prior to construction. Typical materials appear in Table 15-1, and a list of radioactive contaminants appears in Table 15-2.

Table 15-1—Materials used in the construction of detectors

Alumina
Aluminum
Beryllia
Beryllium
Charcoal
Copper
Glass-Epoxy circuit board
Gold
Indium
Lead
Magnesium
Molecular sieve
Polyester, aluminized
Stainless steel
Tin
Tungsten

Table 15-2—Typical radioactive contaminants

Radionuclide	Gamma-ray energy (keV)
^{235}U	186
^{212}Pb	239
^{228}Ac	338
^{208}Tl	583
^{214}Bi	609
^{137}Cs	662
^{228}Ac	911
^{228}Ac	968
^{60}Co	1173
^{60}Co	1332
^{40}K	1461
^{214}Bi	1765
^{214}Bi	2204
^{208}Tl	2614

To further reduce background external to the detector, it can be partially surrounded by a guard detector. A cosmic ray passing through both will produce a signal in the guard that can be used to electrically block the recording of the count from the principal detector. Also, a low-background detector can be surrounded by a lead shield tested to be relatively free of radioactive contaminants. The X-ray background from the lead can be reduced by a graded inner shield, with higher Z materials closest to the lead. Usually, a two-layer shield is adequate: the first layer (next to the lead) is made of cadmium and the second of oxygen-free copper. Other materials may be used.

16. Bibliography

[B1] Bertolini, G. and Coche, A., Ed., *Semiconductor Detectors*, New York: American Elsevier Publishing Company, and Amsterdam: North Holland Publishing Company, 1968.

[B2] Darken, Jr., L. S., Trammell, R. C., Raudorf, T. W., and Pehl, R. H., "Neutron Damage in Ge(HP) Coaxial Detectors," *IEEE Transactions on Nuclear Science*, vol. NS-28, no. 1, pp. 572–578, Feb. 1981.

[B3] Debertin, K. and Helmer, R. G., *Gamma- and X-Ray Spectrometry with Semiconductor Detectors*, New York: North-Holland, 1988.

[B4] Emery, F. E. and Rabson, T. A., *Physical Review*, vol. 140, A2089, 1965.

[B5] Evans, R. D. *The Atomic Nucleus*. Melbourne, Fla.: Krieger Publishing Company, 1982 or New York: McGraw-Hill, 1955.

[B6] Fairstein, E., "Gated Baseline Restorer with Adjustable Asymmetry," *IEEE Transactions on Nuclear Science*, vol. NS 22, no. 1, pp 463–466, Feb. 1975.

[B7] Fairstein, E., "Linear Pulse Shaping Networks: Current Technology," *IEEE Transactions on Nuclear Science*, vol NS 37, no. 2, pp. 382–397, Apr. 1990.

[B8] Ferrari, A. M. R. and Fairstein, E., "Nuclear Preamplifiers and the Pulse Pile-up Problem," *Nuclear Instruments and Methods*, vol. 63, pp. 218–220, 1968.

[B9] Goulding, F. S., "Pulse Shaping in Nuclear Preamplifiers: a Physical Approach to Noise Analysis," *Nuclear Instruments and Measurements*, vol. 100, pp. 493–504, 1972.

[B10] Goulding, F. S., Landis, D. A., and Madden, N. W., "Design Philosophy for High-Resolution Rate and Throughput Spectroscopy Systems," *IEEE Transactions on Nuclear Science*, vol. NS 30, no. 1, pp. 301–310, Feb. 1983.

[B11] Hill, R. F., Hine, G. H., and Marinelli, L. D., "The Quantitative Determination of Gamma-Ray Radiation in Biological Research," *American Journal of Roentgenology, Radium Therapy*, vol. 63, p. 160, 1985.

[B12] Keyser, R., Twomey, T, and Wagner, S. E., "The Benefits of Using Super-Large Germanium Gamma-Ray Detectors for the Determination of Environmental Radionuclides," *Radioactivity and Radiochemistry*, Caretaker Publications, Spring, 1990.

[B13] Knoll, G. F., *Radiation Detection and Measurement*, 2nd. Ed. New York: John Wiley, 1989.

[B14] Kowalski, E., *Nuclear Electronics*, New York, Berlin, Heidelberg: Springer-Verlag, 1970.

[B15] Ottoviani, G., Canali, C., and Alberigi Quaranta, A., "Charge Transport Properties of Semiconductor Materials Suitable for Nuclear Radiation Detectors," *IEEE Transactions on Nuclear Science*, vol. NS 22, no. 1, pp. 192–204 Feb. 1975.

[B16] Paulus, T. J., Raudorf, T. W., Coyne, B., and Trammell, R., "Comparative Timing Performance in Large Volume HPGe Detectors," *IEEE Transactions on Nuclear Science*, vol. NS 28, no. 1, pp. 544–548 Feb. 1981.

[B17] Pehl, R. H., Goulding, F. S., Landis, D. A., and Lenzlinger, M., *Semiconductor Nuclear-Particle Detectors and Circuits*, National Academy of Sciences, Publication 1593, p. 19–36, 1969.

[B18] Radeka, V., "State of the Art of Low Noise Amplifiers for Semiconductor Radiation Detectors," *Proceedings of the International Symposium on Nuclear Electronics*, Versailles, 1968.

[B19] Radeka, V., "Optimum Signal Processing for Pulse-Amplitude Spectrometry in the Presence of High-Rate Effects and Noise," *IEEE Transactions on Nuclear Science*, vol. NS 15, no. 3, pp. 455–476, June 1968.

[B20] Radeka, V., "Trapezoidal Filtering of Signals from Large Germanium Detectors at High Rates," *IEEE Transactions on Nuclear Science*, vol. NS 19, no. 1, pp. 412–428, Feb. 1972.

[B21] *Radiological Health Handbook* (Revised Jan. 1979), available from the U. S. Government Printing Office, Washington, D. C. 20402.

[B22] Raudorf, T. W., Bedwell, M. O., and Paulus, T. J., "Pulse Shape and Risetime Distribution Calculations for HPGe Coaxial Detectors," *IEEE Transactions on Nuclear Science*, vol. NS 29, no. 1, pp. 764–768, Feb. 1982.

[B23] Sakai, E., Malm, H. L., and Fowler, I. L., "Performance of Germanium (Lithium) Detectors Over a Wide Temperature Range," *Semiconductor Nuclear-Particle Detectors and Circuits*, National Academy of Sciences, Publication 1593, p. 101–129, 1969.

[B24] Unterweger, M. P., Hoppes, D. D., and Schima, F. J., "New and Revised Half-Life Measurements Results," *Nuclear Instruments and Measurements in Physics Research*, A312, pp 349–352, 1992.

[B25] Verplanke, J. and Schoenmaekers, W., "New Directions in Germanium Detector Development," *Physica Scripta*, vol. VT32, pp. 218–220 (1990).

[B26] Weast, R. C., Editor, *CRC Handbook of Chemistry and Physics*, 72nd edition, CRC Press, 1992.

Annex A

(informative)

Representative Marinelli beakers[22]

Representative Marinelli beakers are shown in Figure A.1 and its associated table. Note that these are available in addition to the standard Models 450 and 1000 described in 10-6.

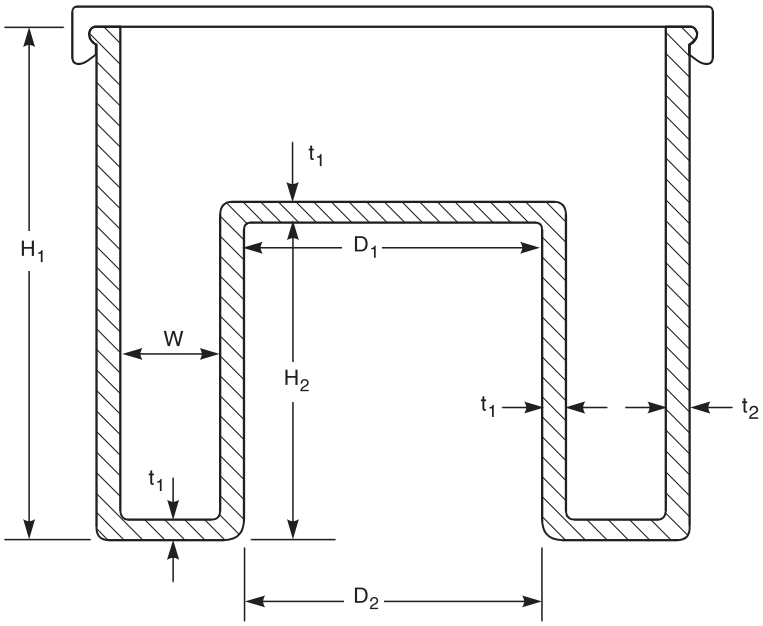

	Volume (mL)[a]		Dimensions						
No.	Nom[b]	Full[c]	H_1 mm (in)	H_2 mm (in)	D_1 mm (in)	D_2 mm (in)	t_1 mm (in)	t_2 mm (in)	W mm (in)
1	675	800	105.4 (4.15)	69.3 (2.73)	58.9 (2.32)	61.0 (2.40)	2.03 (0.08)	2.03 (0.08)	22.4 (0.88)
2	725	1350	152.4 (6.00)	76.2 (3.00)	65.0 (2.56)	67.6 (2.66)	1.52 (0.06)	1.52 (0.06)	22.4 (0.88)
3	495	660	104.1 (4.10)	67.8 (2.67)	71.1 (2.80)	71.6 (2.82)	2.03 (0.08)	2.03 (0.08)	16.8 (0.66)
4	625	815	105.4 (4.15)	67.8 (2.67)	77.5 (3.05)	78.0 (3.07)	2.03 (0.08)	2.03 (0.08)	18.8 (0.74)
5	530	825	117.4 (4.62)	74.7 (2.94)	84.1 (3.31)	86.4 (3.40)	1.78 (0.07)	1.78 (0.07)	13.7 (0.54)
6	680	720	117.4 (4.62)	95.5 (3.76)	81.0 (3.19)	82.3 (3.24)	1.78 (0.07)	1.78 (0.07)	15.7 (0.62)
7	405	720	117.4 (4.62)	76.5 (3.01)	91.4 (3.60)	93.2 (3.67)	1.78 (0.07)	1.78 (0.07)	10.2 (0.40)
8	1265	1950	165.6 (6.52)	101.1 (3.98)	96.5 (3.80)	98.0 (3.86)	1.52 (0.06)	1.52 (0.06)	21.8 (0.86)
9	1105	1855	165.9 (6.53)	101.4 (3.99)	103.6 (4.08)	105.7 (4.16)	1.27 (0.05)	1.52 (0.06)	18.3 (0.72)
10	2670	3700	177.3 (6.98)	104.9 (4.13)	113.8 (4.48)	116.6 (4.59)	1.52 (0.06)	1.52 (0.06)	32.8 (1.29)

[a]The volumes were computed from the dimensions, then rounded to the nearest 5 mL.
[b]When filled to the nominal volume, the top surface of the solution will be $H_2 + W_{ave} + t_1$ above the bottom of the beaker, i.e., above the plane of the reentrant region by a distance equal to the average thickness of the annulus.
[c]Full volume is the maximum volume.

Figure A.1—Some representative Marinelli (reentrant) beakers

[22]Potential suppliers for standard 450 mL and 1000 mL Marinelli beakers are Bel-Art products, Central Molding Corporation, GA-MA Associates, and New England Nuclear. Potential suppliers for sealed beakers filled with radioactive materials are APT (Applied Physical Technology), Amersham Corporation, Isotopes Products Laboratories, and New England Nuclear.